OPEN ACCESS

University of BRISTOL

Dong, Q., Meng, Z., Ho, C-L., Guo, H., Wang, W., Manners, I., Xu, L., & Wong, W-Y. (2018). A molecular approach to magnetic metallic nanostructures from metallopolymer precursors. *Chemical Society Reviews*, *47*(13), 4934-4953. https://doi.org/10.1039/c7cs00599g

Peer reviewed version

License (if available):
Unspecified

Link to published version (if available):
10.1039/c7cs00599g

Link to publication record in Explore Bristol Research
PDF-document

This is the author accepted manuscript (AAM). The final published version (version of record) is available online via Royal Soc. of Chemistry at https://pubs.rsc.org/en/content/articlehtml/2018/cs/c7cs00599g. Please refer to any applicable terms of use of the publisher.

University of Bristol - Explore Bristol Research
General rights

This document is made available in accordance with publisher policies. Please cite only the published version using the reference above. Full terms of use are available:
http://www.bristol.ac.uk/red/research-policy/pure/user-guides/ebr-terms/

A molecular approach to magnetic metallic nanostructures from metallopolymer precursors

Qingchen Dong,[*a¥] Zhengong Meng,[b¥] Cheuk-Lam Ho,[*cd] Hongen Guo,[a] Weiyou Yang,[*e] Ian Manners,[*f] Linli Xu,[c] Wai-Yeung Wong[*cd]

[a] *MOE Key Laboratory for Interface Science and Engineering in Advanced Materials and Research Center of Advanced Materials Science and Technology, Taiyuan University of Technology, 79 Yingze West Street, Taiyuan 030024, P.R. China.*
[b] *School of Chemistry and Environmental Engineering, Shenzhen University, Shenzhen 518060, P.R. China.*
[c] *Department of Applied Biology and Chemical Technology, The Hong Kong Polytechnic University, Hung Hom, Hong Kong, P.R. China and The Hong Kong Polytechnic University Shenzhen Research Institute, Shenzhen, P.R. China.*
[d] *Institute of Molecular Functional Materials and Department of Chemistry, Hong Kong Baptist University, Waterloo Road, Kowloon Tong, Hong Kong, P.R. China and HKBU Institute of Research and Continuing Education, Shenzhen Virtual University Park, Shenzhen 518057, P.R. China.*
[e] *Institute of Materials, Ningbo University of Technology, Ningbo 315016, P.R. China.*
[f] *School of Chemistry, University of Bristol, Bristol BS8 1TS, UK.*

Corresponding authors

* E-mail: dongqingchen@tyut.edu.cn; cheuk-lam.ho@polyu.edu.hk; weiyouyang@tsinghua.org.cn; Ian.Manners@bristol.ac.uk; wai-yeung.wong@polyu.edu.hk

[¥] They contributed equally to this work.

Qingchen Dong obtained her Ph.D. degree under the tutelage of Prof. Wai-Yeung Wong in 2012 at Hong Kong Baptist University (HKBU). She also worked at Caltech with Prof. H. B. Gray from 2010 to 2011. She is a professor of Taiyuan University of Technology (TYUT). Her research involves the synthesis of functional metallopolymers and magnetic nanocomposites for applications in data storage, optoelectronics, catalysis and biomedicine.

Zhengong Meng obtained his Ph.D. degree at HKBU in 2016. He is currently an associate professor at Shenzhen University. His research focuses on magnetic alloy nanoparticles for high-density magnetic recording.

Cheuk-Lam Ho earned her Ph.D. degree from HKBU in 2007. She is currently an assistant professor at the Hong Kong Polytechnic University (PolyU) and her research interest is in functional metallophosphors and metallopolymers for light-emitting and photovoltaic applications.

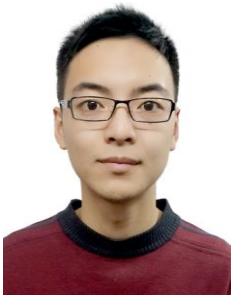

Hongen Guo is now a graduate student of TYUT under the supervision of Prof. Qingchen Dong. His research mainly focuses on the synthesis and applications of functional metallopolymers.

Weiyou Yang received his Ph.D. degree in Materials Science and Engineering from Tsinghua University in 2005. He works in Ningbo University of Technology, and is currently the leader of Institute of

Materials there. His research lies in the field of controlled growth, properties and applications of low-dimensional nanostructures.

Ian Manners received his Ph.D. from the University of Bristol and conducted postdoctoral works in Germany and USA. He joined the University of Toronto in 1990, and after 15 years returned to his Alma Mater to take up a Chair in Inorganic, Macromolecular and Materials Chemistry. His research interests focus on the development of new synthetic reactions and self-assembly protocols and their applications in molecular synthesis, polymer/materials science, and nanoscience.

Linli Xu obtained her Ph.D. degree from Guangzhou Institute of Chemistry, Chinese Academy of Sciences (CAS) in 2010. She then carried out research at Technical Institute of Physics and Chemistry, CAS, from 2012 to 2017. She now works at PolyU as a research fellow and her research focuses on polymer materials and carbon materials.

Wai-Yeung Wong obtained his Ph.D. degree from the University of Hong Kong. He did postdoctoral works at Texas A&M University and University of Cambridge. He joined HKBU from 1998 to 2016 and he now works at PolyU as Chair Professor of Chemical Technology and Associate Dean of Faculty of Applied Science and Textiles. His research focuses on synthetic inorganic/organometallic chemistry, especially aiming at developing metal-organic molecules and polymers for organic optoelectronics and metal-based nanomaterials.

Abstract: In recent years, metallopolymers have attracted much attention as precursors to generate magnetic metal/metal alloy nanoparticles (NPs) through pyrolysis or photolysis because they offer the advantages of ease of solution processability, atomic level mixing and stoichiometric control over composition. The as-generated NPs usually hold narrow size distributions with precise control of composition and density per unit area. Moreover, patterned NPs can be achieved on various substrates in this way owing to the good film-forming property of metallopolymers and such work is important for many applications based on metal nanostructures. By combining the merits of both the solution processability of metallopolymers and nanoimprint lithography (NIL), a new platform can be created for fabricating bit-patterned media (BPM) and next-generation of nanoscale ultra-high-density magnetic data storage devices. Furthermore, most of these metallopolymers can be used directly as a negative-tone resist to generate magnetic metallic nanostructures by electron-beam lithography and UV photolithography. Self-assembly and subsequent pyrolysis of metalloblock copolymers can also afford well-patterned magnetic metal or metal alloy NPs *in situ* with periodicity down to dozens of nanometers. In this review, we highlight on the use of metallopolymer precursors toward synthesizing magnetic metal/metal alloy NPs and their nanostructures and the related applications.

Key learning points

(1) Classification and general synthetic procedures of metallopolymer precursors for the synthesis of magnetic metal/metal alloy nanoparticles (NPs).

(2) Fabrication techniques of magnetic nanopatterned arrays.

(3) Applications of the as-synthesized magnetic metal/metal alloy NPs.

(4) Key challenges and opportunities of functional nanomaterials from metallopolymer precursors.

1. Introduction

Magnetic nanoparticles (MNPs) with size down to 2-20 nm are of great interest because each NP is equivalent to a single magnetic domain, which results in two significantly different types of magnetic behaviors in NPs: single domain ferromagnetic and superparamagnetic.[1] Generally speaking, the magnetic behavior of NPs is closely related to their size, composition and temperature. Due to the special magnetic property of magnetic NPs in comparison to their counterparts in bulk, they can be applied in different areas, for instance, ferromagnetic NPs for data recording and permanent magnets, and superparamagnetic NPs for targeted drug delivery, hyperthermia and magnetic resonance imaging (MRI), *etc*.[2-7] Therefore, various methods have been explored to synthesize MNPs, such as physical deposition, gas-phase evaporation, solution-phase synthesis, *etc*. Among these MNPs, magnetic alloy NPs are particularly interesting due to their high saturation magnetization and chemical stability, which can be synthesized through vacuum-deposition techniques, reduction or thermal decomposition of two separated metal sources or single bimetallic carbonyl clusters, *etc*.[8] However, there are still some undesirable problems concomitant with the above synthetic approaches: i) sophisticated instrument and complicated procedures are needed for vacuum-deposition and gas-phase evaporation techniques,

which are also quite time-consuming; ii) problems such as agglomeration, sintering and broad particle size distribution, *etc.* are inevitable in the post-annealing treatment of solution-phase synthesis.[2,4] Therefore, direct and facile synthesis of MNPs with specific crystalline phase (especially for the ferromagnetic alloy NPs) and low size distribution is urgently needed for the practical application of magnetic metal/metal alloy NPs. More importantly, ordered arrays of magnetic nanostructures with unique physical traits are very desirable in areas such as biosensors, spintronics, magnetic random access memory (MRAM), and patterned recording media, whereas conventional synthetic methods of MNPs are not suitable for the direct and rapid fabrication of patterned magnetic nanostructure with high areal density and in large area.[2,3]

Metallopolymers with metal centers incorporated in the polymer backbone are emerging as an interesting and important class of easily processable materials with attractive properties and functions, which have attracted wide research interest in multiple disciplines.[9] In recent years, metallopolymers as precursors to generate metal/metal alloy nanocomposites have aroused considerable attention because they offer the advantages of ease of solution processability, atomic level mixing and stoichiometric control over composition. Particularly, their use as precursors for synthesizing magnetic metal/metal alloy NPs by thermal or radiation treatment is intriguing.[2,3,10] The as-generated MNPs usually possess narrow size distributions with precisely controllable composition and density per unit area. Moreover, patterned NPs over large areas can be achieved on various substrates in this way owing to the good

film-forming property of metallopolymers and such work is important for many applications based on metal nanostructures. The major advances, ongoing challenges and future perspectives of such research are described in this review.

2. Metallopolymer precursors

Since the first metal-containing polymer, poly(vinylferrocene), was synthesized and reported in 1955, metallopolymers with metal centers incorporated in the polymer chains have gradually developed as one of the most exciting functional materials accompanied by the discovery of new synthetic approaches, such as living polymerization, metal-catalyzed ring-opening metathesis polymerization, ring-opening photopolymerization, electropolymerization, metal-catalyzed coupling reactions, *etc*.[9] Metallopolymers are generally polymers with one or several kinds of metal elements located in side chain and/or backbone of the polymers. The introduction of metal ions endows the polymer many significant advantages: i) organic functional subunits can be assembled together through coupling with metal ions; ii) the electronic and optical properties of organic conjugated systems can be changed through the interaction of metal d-orbitals with the ligand orbitals; iii) various molecular frameworks can be achieved according to the coordination number, geometry and valence states of metal atoms.[11] Therefore, metallopolymers with different metal elements and geometries display a diversity of structures and properties, thus leading to versatile applications. For example, metallopolymers with reversible redox properties are of interest for nano-electronics, electrocatalysis, information storage, nanopatterning, sensing, and also as responsive surfaces and capsules, active components of photonic crystal

displays, emissive and photovoltaic materials, optical limiters and artificial enzymes, *etc*.[12-17] More recently, as discussed above, metallopoymers have been used for preparation of magnetic NPs with desired phase, composition and patterned nanostructures.

2.1 Design and synthesis of metallopolymer precursors

A precise control of the structure of metallopolymer is very crucial, because it is closely related to the size, composition and properties of the resultant magnetic ceramic NPs. According to the position and identity of metal atoms in the backbone of polymers, metallopolymers can be classified into different types, e.g. polymers containing metal elements in the side chain or main chain; heterobimetallic or mononuclear metallic polymers, *etc*. Fig. 1 is a cartoon illustration of several typical structures of heterobimetallic and mononuclear metallic polymers with metal elements in the side chain and/or main chain. Normally, cyclopentadienyl compounds such as ferrocene, cobaltocenium ion, *etc*. as metal sources are introduced into the side chain of the polymer backbone. For main-chain metallopolymers, strained [*n*]metallocenophanes and their analogues can be used to yield high-molecular-weight main-chain metallopolymers through ring-opening polymerization (ROP) reaction. By employing the diblock or block-random copolymers (with the general structure of A-*b*-(B-*r*-C)) as precursors, one can control the metal content and metal atom ratios easily by changing the molar ratio of monomers. Moreover, in order to increase the ceramic yields, metallopolymers with cross-linked structure is an effective way due to the decrease of volatile decomposition products in the pyrolysis process.[9,12]

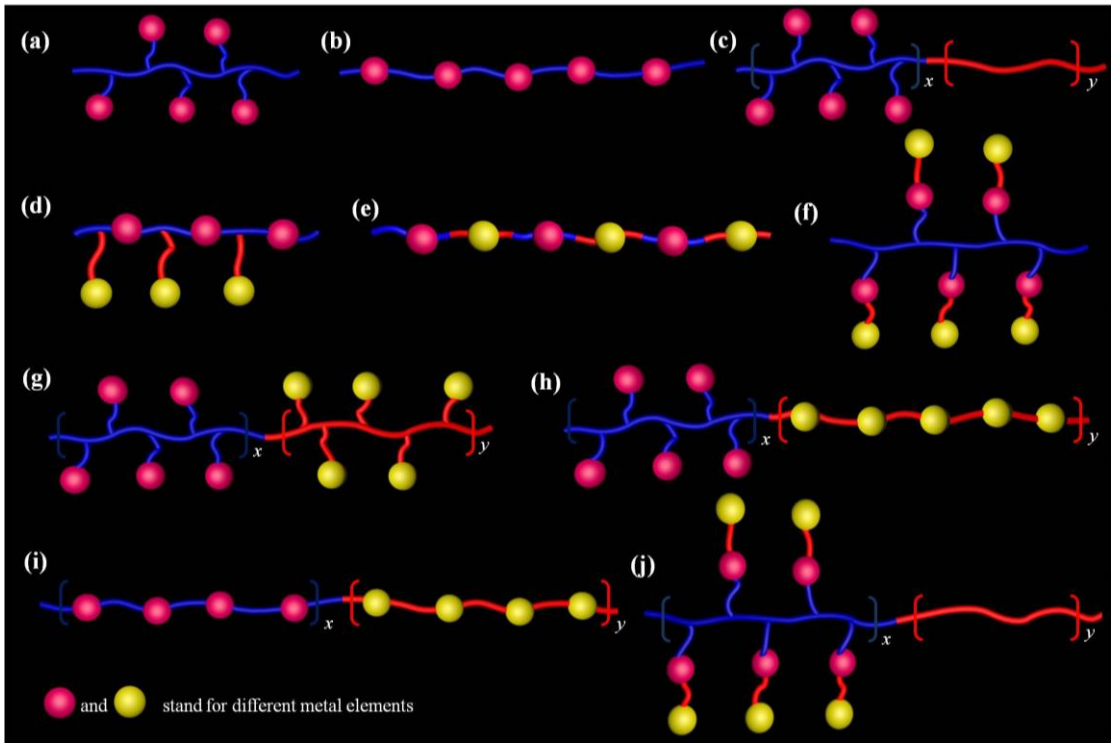

Fig. 1 Cartoon illustration of the structures of typical mononuclear metallic (a-c) and heterobimetallic (d-j) polymer precursors.

More recently, a review for the synthetic approaches of metallopolymers (especially for the Co-containing polymers) has been reported by Astruc and Gu, *et al.*,[9] which summarizes the radical polymerization, reversible-addition-fragmentation chain transfer (RAFT), post-polymerization, atom transfer radical polymerization (ATRP), and ring-opening metathesis polymerization (ROMP), *etc*. Because of the space limitation of this review, the details of the above polymerization reactions will not be discussed here. The majority of polyplatinaynes as described in this review were prepared by the Hagihara's dehydrohalogenation reaction. In a typical Hagihara's dehydrohalogenation reaction, platinum(II) halide complex $[PtL_2Cl_2]$ and diethynylarylene ligands (HC≡CArC≡CH) can be cross-coupled together in the presence of cuprous halide and amine, which act as the catalyst and acid

acceptor/solvent, respectively, and the polymerization can proceed efficiently at room temperature. By employing the Hagihara cross-coupling reaction, nearly equiatomic ratio of two metal elements in the side chain and/or main chain of heterobimetallic polymers can be achieved.[11] Moreover, the long alkyl chains are often introduced to increase the solubility of the resultant metallopolymer, which is very desirable for the nanopatterning by solution process. The chemical structures, molecular weight and thermal properties of these metallopolymers were typically characterized by nuclear magnetic resonance (NMR), infrared (IR), ultraviolet-visible (UV-vis) spectroscopic methods, elemental analysis (EA), gel permeation chromatography (GPC), differential scanning calorimetry (DSC), and thermal gravimetric analysis (TGA), *etc*.

2.2 Heterobimetallic polymer precursors

2.2.1 FePt-containing and CoPt-containing heterobimetallic polymers

Iron-platinum alloy NPs have drawn extensive attention because of their remarkable magnetic properties, which can be generated from FePt-containing metallopolymer precursors through the single-step pyrolysis.[2,3,18] Initially, some polyferroplatinynes with phosphine ligands on Pt (e.g. **P1** in Fig. 2) were used which are not suitable for the synthesis of pure $L1_0$-FePt NPs because the unwanted phases of Fe_2P and PtP_2 are co-generated.[2] To avoid this, a series of bimetallic polyferroplatinynes **(P2–P6)** with 4,4'-dinonyl-2,2'-bipyridine were synthesized instead. Pure ferromagnetic $L1_0$-FePt NPs were formed directly from **P2–P6** through pyrolysis without any post-annealing treatment. All these *N, N'*-coordinated polyplatinynes were synthesized with satisfactory yields according to the

CuI-catalyzed Hagihara's dehydrohalogenation reaction of a diethynylarylene ligand with *cis*-[$PtCl_2$(diimine)] (Scheme 1).[2,11,16,19] In 2016, a new synthetic pathway of heterobimetallic polymer (**P7**) through grafting FePt-containing ligand onto the backbone of a random copolymer poly(ethynylstyrene-styrene) was reported.[20] Moreover, by taking advantage of the templating effect of the porphyrin derivatives, different metal atoms were introduced into the macrocyclic center of porphyrin ligands which can then be coupled with the other ligand to generate a series of porphyrin-based metallopolymers with either one or both metal elements in the main chain. **P8** and **P9** are two porphyrin-based FePt-containing and CoPt-containing metallopolymers, which are synthesized by coupling of the diethynyl Fe^{III}-porphyrin or diethynyl Co^{II}-porphyrin ligand with *cis*-[$PtCl_2$(diimine)].[21,22] Usually, these FePt-containing metallopolymers were purified through repeated precipitation in a minimum volume of dichloromethane from methanol for several times to remove away any inorganic catalysts and the low-molecular-weight species. Their structures and thermal properties can be characterized by NMR, IR and TGA, *etc*. IR spectral analysis is particularly important for the identification of polymers with low solubility. The existence of peak at around 2100 cm^{-1} corresponding to the stretching vibrational frequency of C≡C and disappearance of the terminal C≡C–H bond stretching vibration frequency at around 3300 cm^{-1} can verify that all the alkynyl ligands and metal fragments were coupled together. Most of these polymers are air stable and show excellent thermal stability with the onset decomposition temperature (T_{decomp}) higher than 300 °C.

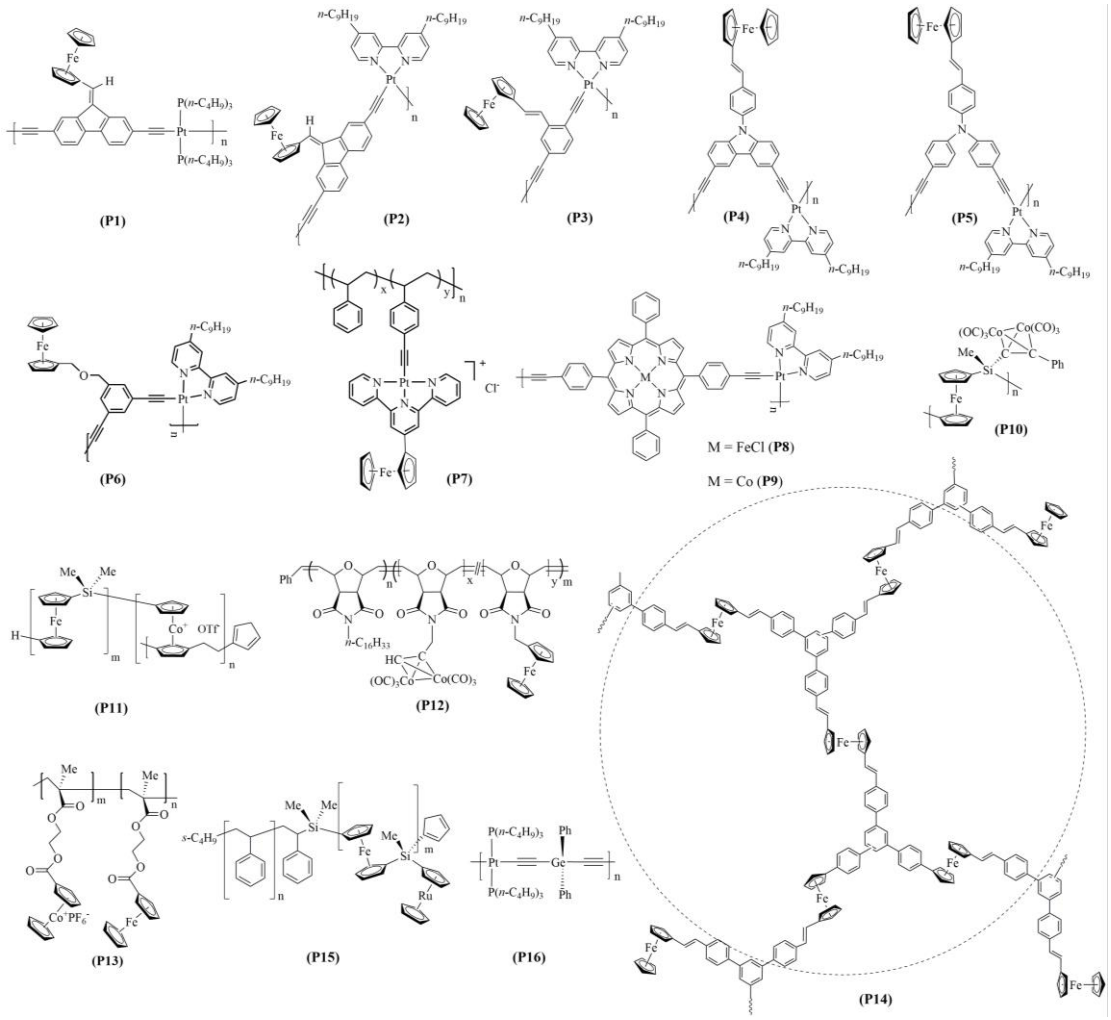

Fig. 2 Chemical structures of heterobimetallic polymer precursors.

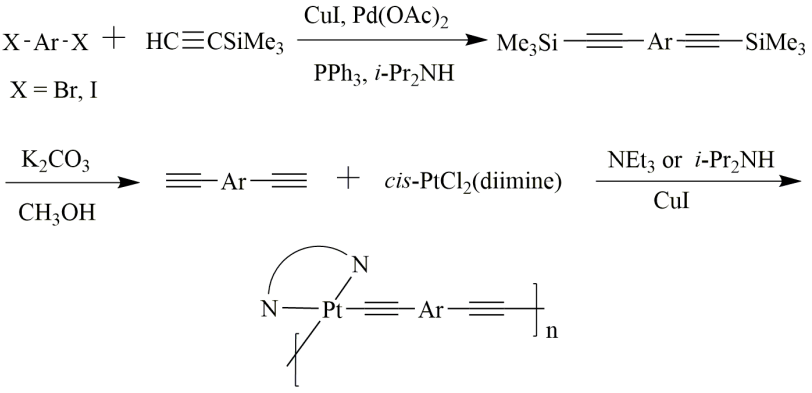

Scheme 1 General synthetic strategy of *N*, *N*'-coordinated polyplatinynes.

2.2.2 CoFe-containing heterobimetallic polymers

The CoFe-containing polymers **P10** and **P11** were also synthesized, which can afford CoFe metal alloy NPs through controlled pyrolysis.[10,23,24] For **P10**, an

acetylene-substituted polyferrocenylsilane (PFS) intermediate was prepared, which then reacted with [$Co_2(CO)_8$] to provide a CoFe-containing polymer in high yield with Fe atoms in the main chain and Co atoms in the side chain.[23] The thermal gravimetric analysis was performed to evaluate the thermal stability, indicating that the T_{decomp} of **P10** is 320 ^oC. Metal-containing diblock or triblock copolymers have been widely studied because they offer a simple, alternative approach to allow nanopatterning of functional metal/metal alloy NPs as a result of their ability to undergo self-assembly in the solid state or solution (*vide infra*). **P11** is actually a polyferrocenylsilane-*b*-poly(cobaltoceniumethylene) block copolymer (PFS-*b*-$[PCE]^+$) synthesized by sequential photo-controlled ROP of sila[1]ferrocenophane and dicarba[2]cobaltocenophane followed by oxidation of the 19-electron cobaltocene.[24] The structure and thermal properties of **P11** were characterized by NMR, DSC and TGA, respectively. The glass-transition temperature (T_g) and T_{decomp} of **P11** are determined to be around 33 and 340 ^oC, respectively. Tew *et al*. demonstrated a series of CoFe-containing block-random copolymers composed of a well-defined alkyl-functionalized (C_{16}) homoblock and a random block with cobalt complex- (Co) and ferrocene-functionalized (Fe) moieties (C_{16}-*b*-(Co-*r*-Fe)) (**P12**) through stepwise ROMP reaction.[13] The volume fraction of the random block (Co-*r*-Fe) was held constant to maintain the same cylindrical morphology after phase separation for all the block-random copolymers with different ratios of Co and Fe monomers. The molecular structure and weight of **P12** were characterized by NMR and GPC, respectively, indicating the number-average molecular weight of **P12** is in the range of 82-100 kDa.

Moreover, the authors also found that the magnetic properties of the block copolymer nanostructures as formed by solvent annealing of **P12** is dependent of the molar ratio of the Co units to the Fe units in the random block. In 2014, Tang and co-workers reported the preparation of cobaltocenium/ferrocene-containing heterobimetallic block copolymers (**P13**).[6] The cobaltocenium-containing homopolymer with hexafluorophosphate as counterion was first synthesized through RAFT polymerization. Then ferrocene-containing methacrylate monomers were chain-extended from the cobaltocenium-containing homopolymer to form heterbimetallic diclock copolymers. By varying the ratios of two monomers, the length of ferrocene block can be controlled, which can be confirmed by ^{1}H NMR spectra.

Tang *et al.* reported the synthesis of hyperbranched conjugated poly(ferrocenylphenylenes) (*hb*-PFPs) (**P14**) through the copolycyclotrimerization of diynes.[25] These polymers are soluble, thermally-stable and redox-active. Further complexation of *hb*-PFPs with [$Co_2(CO)_8$], namely post-polymerization, gave FeCo-containing heterobimetallic polymers.

2.2.3 Others

Sila[1]ferrocenophanes are a class of ring-strained organometallic molecules that undergo ROP to afford PFSs. This is a photolytic ROP reaction which is tolerant of groups other than alkyl chains at silicon, and enables the preparation of PFSs with an alkynyl pendant. The subsequent macromolecular clusterization of the triple bonds with homonuclear transition-metal then afforded mixed-metal metallopolymers of iron and molybdenum or nickel.[26]

The use of pendant metallocenes to incorporate elements other than Fe into PFSs is proved to be an effective route to mixed-metal metallopolymers. For ruthenocenylsila[1]ferrocenophane (**P15**), the ratio of metallic elements may be controlled by the stoichiometry of the monomer rather than by the efficiency of any post-polymerization step.[27] Recently, another thermally-stable polymeric Pt-based germylacetylene **(P16)** was also prepared.[28]

2.3 Mononuclear metallopolymer precursors

To overcome the practical limitations (e.g. poor solubility, synthetic difficulty, *etc.*) of heterobimetallic polymers, patterned metal alloy NPs can also be produced by blending two individual homopolymers with equiatomic ratio of the metal atoms, followed by pyrolysis of the resulting nanopatterned polymer blend (as shown in Fig. 3). Both homopolymers are more soluble in organic solvents and easy to synthesize in comparison to their binary-metal-containing counterparts.

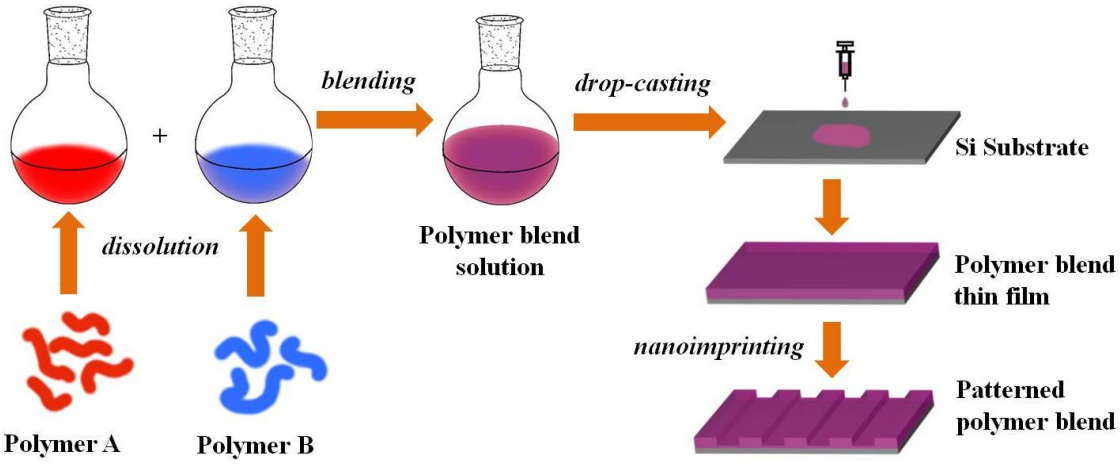

Fig. 3 A diagram showing the formation of the polymer blend of two mononuclear metallopolymers useful for subsequent patterning studies.

2.3.1 Fe-containing and Pt-containing homopolyynes

The synthesis of Pt-containing metallopolymer (**P17**) and Fe-containing

metallopolymer (**P18**) (Fig. 4) was reported.[29] **P17** was synthesized by the CuI-catalyzed dehydrohalogenation reaction between 2,7-diethynyl-9,9'-didodecylhexylfluorene and *cis*-[Pt(diimine)Cl_2]. **P18** was made from a Sonogashira coupling reaction of 2,7-diiodo-9,9'-didodecylhexylfluorene with a ferrocene-anchored diethynyl ligand. One can easily design and synthesize different Fe-containing metallopolymers by introducing a ferrocenyl moiety into the polymer backbone. **P19** is a Pt-containing metallopolymer which can be prepared through the Sonogashira coupling of diethynyl Pt^{II}-porphyrin compound and diiodofluorene ligand.[30] All these monometallic polymers are air-stable and soluble in common organic solvents, and are thus suitable for patterning studies by solution-processing methods.

2.3.2 PFS and analogues

ROP reactions of strained [*n*]metallocenophanes and their analogues with related C_x (x = 4–7) π-hydrocarbon ligands can be used to yield high-molecular-weight main-chain metallopolymers, and the strain, which acts as a thermodynamic driving force for ring-opening, is related to the tilt angle in addition to other structural parameters.[31] PFS, which is prepared by ROP of silicon-bridged [1]ferrocenophanes, has drawn much interest as redox-responsive films, gels, capsules, nanostructured magnetic film precursors, etch resists for nanolithography and patternable sources of carbon nanotube growth catalysts.[32] **P20**, **P21** and **P22** are typical examples of processable high-molecular-weight PFSs. Likewise, metallopolymers based on other metals such as Co, Ni, Ti, V and Cr have also been prepared by ROP of relevant

strained precursors.[33,34] For example, green-colored soluble poly(nickelocenylpropylene) **(P23)** was generated by ROP of tricarba[3]nickelocenophane in pyridine at room temperature.[33] Moreover, ferrocene or cobaltocenium hexafluorophosphate-containing block copolymers (**P24** and **P25)** with metal elements in the side chain have also been synthesized through the RAFT, ATRP, ROMP, radical polymerization and post-polymerization approaches by Tang and Astruc, *etc.* Most of these polymers are soluble and show interesting redox properties.[6,9,13]

2.3.3 Co-containing metallopolymers

Bunz *et al.* reported the synthesis of main-chain organometallic poly(*p*-phenyleneethynylene) (PPE) through metalation of PPE with $[Co_2(CO)_8]$. However, most of these metallopolymers exhibit poor solubility except for **P26**, which has long octyl groups on the phenyl rings.[35]

Tang and co-workers prepared some carbon-rich hyperbranched polyynes (*hb*-PYs) (**P27**) through copolycyclotrimerization of triynes, which are readily curable, thermally-stable and pyrolytically carbonizable. Complexation of the triple bonds in *hb*-PYs with $[Co_2(CO)_8]$ afforded the cobalt-polyyne polymers.[36] Recently, Grubbs and co-workers showed that block copolymers with analogous Co clusters in one segment afforded Co NPs confined to the organometallic nanodomains on mild thermal treatment (120 °C).[37] **P28** is a porphyrin-based Co-containing metallopolymer synthesized similar to that of **P19**.[38]

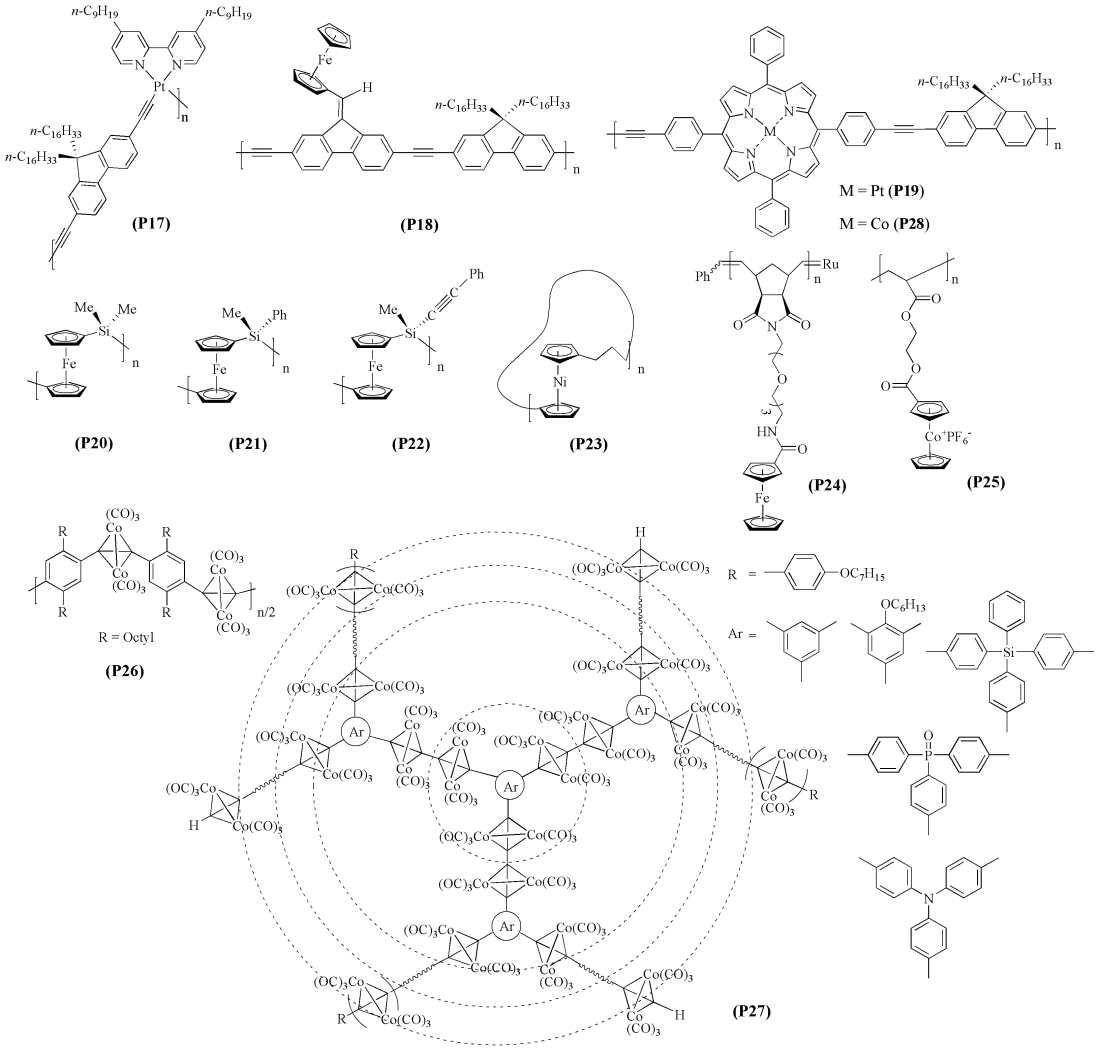

Fig. 4 Chemical structures of mononuclear metallopolymer precursors.

3 Metallopolymer precursors to magnetic metal/metal alloy NPs

Recently, researchers have attempted to synthesize metal/metal alloy NPs by utilizing metallopolymers as templates which, on pyrolysis or photolysis, generate NPs with narrow size distribution and precisely controllable composition as well as density per unit area. Metallopolymers are typically pyrolyzed in a tube furnace, which is purged with an inert or a reductive gas atmosphere and heated to the desired temperature at a heating rate for a certain period to give black NPs. Moreover, patterned NPs can be obtained on various substrates in this way owing to the favorable

film-forming feature of metallopolymers. Before the discussion of the synthesis of magnetic NPs from metallopolymer precursors, a brief introduction of nanomagnetism is provided first to allow a clear understanding of the magnetic properties of nanomaterials as discussed in this review.

3.1 Basic knowledge of nanomagnetism

As mentioned above, MNPs with size down to 2−20 nm can display single-domain ferromagnetic and superparamagnetic behaviors. This special feature of MNPs is mainly dominated by two issues: finite size and surface effects. The most investigated finite size effects in MNPs include the single-domain limit, superparamagnetic limit, and disappearance of coercivity (H_c).[1,5]

In contrast to their counterparts in the bulk (comprised of multiple magnetic domains), MNP can behave as a single magnetic domain when it is reduced down to a critical size, which is denoted as the single-domain limit. This limit is closely related to the composition and crystal structure of MNPs. The critical diameter for a magnetic particle to reach the single-domain limit is defined by

$$R_{sd} = \frac{36\sqrt{AK}}{\mu_0 M_s^2} \quad (1)$$

where A is the exchange constant, K is the effective anisotropy constant and M_s is the saturation magnetization. For most magnetic materials, this diameter is in the range of 10−100 nm and except for some high-anisotropy materials, the single-domain limit can be several hundred nanometers. If the size of a ferromagnetic NP is further reduced, it eventually reaches the superparamagnetic limit. Below this limit, the magnetic spin of

NPs can randomly flip due to thermal fluctuation, leading to a zero net magnetization and the NPs are superparamagnetic. Fig. 5 shows a schematic diagram illustrating the magnetic behaviors of an array of single-domain MNPs in the block state and an array of superparamagnetic NPs. It can be seen clearly that the ferromagnetic NPs in Fig. 5a can be magnetized to reach saturation by applying an external magnetic field which is strong enough, and the corresponding moment is called the saturation moment (M_s). When the external field is removed, the ferromagnetic NPs retain a considerable degree of magnetization which is referred as the remnant magnetic moment (M_r). Thanks to this remnance of magnetic moment, magnetic memory devices with MNPs can be developed.[4] To demagnetize the particles, the external field with reversed orientation should be applied. The magnetic field intensity as required to demagnetize the magnetic moment of NPs from saturation to zero is called coercivity. For application in magnetic recording storage, the magnetic domains should have an appropriate value of H_c which is high enough to protect against thermal fluctuation, but low enough for information writing. At present, MNPs with H_c in the range of 2.5-3.1 kOe are thought to be suitable for disk drive media. The coercivity is strongly related to the magnetic anisotropy constant (K_u) and particle size (V), which can be defined by

$$H_c = 2K_u m_s^{-1}(1 - 5\sqrt{kT/K_u V})^{-1} \quad (2)$$

For the superparamagnetic NPs in Fig. 5b, the NPs can be magnetized to saturated state fast and then randomized to zero after the external field is removed due to thermal fluctuation. Thus, no hysteresis appears in the magnetization curve. Superparamagnetic NPs have a relatively small energy barrier ($K_u V$) to the change of the magnetic spin

direction in comparison to ferromagnetic NPs. As the size of a NP is reduced, the energy barrier is comparable to the thermal energy, k_BT, and the transition will occur from ferromagnetic to superparamagnetic. This transition temperature is named as the blocking temperature, T_b, given by

$$T_b = K_uV/25k_B \quad (3)$$

where K_u is the uniaxial magnetic anisotropy constant, V is the particle volume, and k_B is the Boltzmann constant. Due to the large constant magnetic moment, fast response to applied magnetic fields, negligible remnant moment and agglomeration, the superparamagnetic NPs are very intriguing in biomedical applications. The magnetic properties of NPs can be characterized by many techniques, such as superconducting quantum interference device (SQUID), vibrating sample magnetometry (VSM), and X-ray magnetic circular dichroism (XMCD), *etc*.[5]

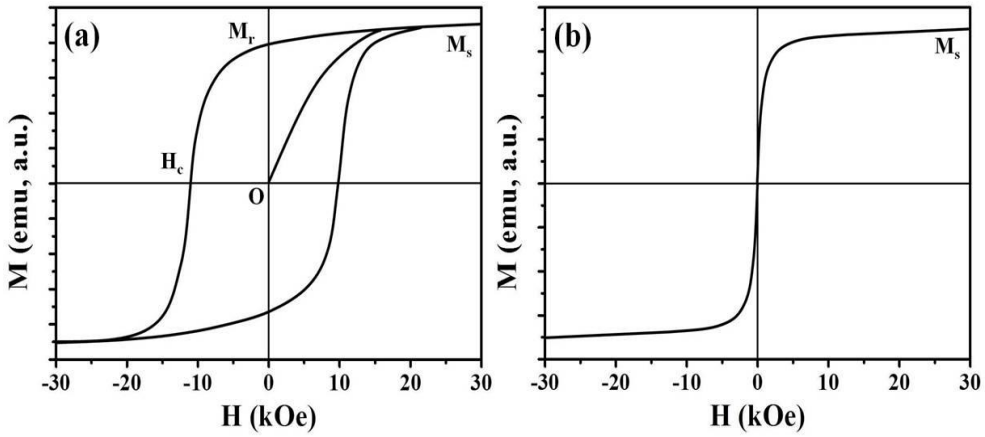

Fig. 5 Schematic illustration of (a) a typical magnetic hysteresis loop of an array of single-domain ferromagnetic NPs and (b) a typical *M-H* curve of a group of superparamagnetic NPs.

3.2 FePt and CoPt NPs

As far as the ultra-high-density magnetic data recording is concerned, the superparamagnetic limit is a significant challenge, because reliable recording must

satisfy the thermal stability condition of $K_uV/k_BT > 60$. Therefore, it is very desirable for exploring NPs with a large K_u, while maintaining a compact V at room temperature. Bimetallic alloys composed of 3d magnetic elements and 5d (or 4d) elements, such as FePt, FePd, CoPt, Co_3Pt, *etc.*, have attracted wide research interest in the field of magnetic data storage, as a consequence of their high thermal stability due to the spin-orbit coupling and hybridization of 3d and 5d electrons. Among these, ferromagnetic FePt and CoPt NPs are very attractive for fabricating the ultra-high-density magnetic data storage media, because of their high chemical stability and extraordinarily large uniaxial magnetocrystalline anisotropy K_u in the bulk phase.[3] Table 1 lists the properties of some ferromagnetic metal alloy materials.[39] Two common phases exist for FePt and CoPt alloy NPs, viz., the more chemically ordered face-centered tetragonal (fct or $L1_0$) and the less ordered face-centered cubic (fcc or A_1) phases (see Fig. 6). The $L1_0$ FePt or CoPt NPs are ferromagnetic, while the A_1 phase is superparamagnetic. Usually, the A_1 phase FePt or CoPt NPs can be transformed to the $L1_0$ phase by thermal treatment. The most common synthetic methods for the preparation of $L1_0$ FePt NPs generally involve two steps: firstly, the mixture of separated Fe- and Pt-sources, which are usually inorganic chemical reagents, is refluxed in a high-boiling organic solvent to give rise to superparamagnetic A_1 phase FePt NPs; secondly, the resulting A_1 phase FePt NPs are thermally annealed to give the desired ferromagnetic $L1_0$ phase. However, undesirable defects such as agglomeration, sintering and broad particle size distribution are inevitably concomitant with this method, due to the fact that the elements Fe and Pt are originally present in separate

compounds which have different onset decomposition temperatures. Although several FePt-containing organometallic complexes as single-source precursors were explored and used to directly synthesize $L1_0$ phase FePt NPs, this is unfavorable for data storage devices because direct and rapid fabrication of patterned $L1_0$-FePt nanostructure is indispensable in realizing data storage systems.[7,29] In 2012, the direct one-step synthesis of $L1_0$-FePt NPs from **P3** was described.[3] The morphology, composition and magnetic property of the resulting FePt NPs were investigated by transmission electron microscopy (TEM), powder X-ray diffraction (PXRD), energy-dispersive X-ray (EDX) elemental analysis and VSM, indicating that the as-generated FePt NPs are $L1_0$ phase ferromagnetic alloy NPs with the atomic ratio of Fe to Pt close to 50 : 50 and average size of 4.6 nm. To overcome the limitations (e.g. poor solubility (not suitable for nanopatterning), synthetic difficulty, *etc.*) of heterobimetallic polymers, the facile generation of $L1_0$-FePt NPs with a narrow size distribution (average size ~4.9 nm) was reported by blending two individual Pt-containing (**P17**) and Fe-containing (**P18**) homopolymers with equiatomic ratio of Pt and Fe, followed by controlled pyrolysis of the resulting polymer blend to give $L1_0$-FePt NPs.[29] Generally, homopolymers exhibit better solubility in organic solvents and are easy to synthesize in comparison to the binary-metal-containing metallopolymers (e.g. **P2** and **P3**). The TEM images of the as-synthesized $L1_0$-FePt NPs are depicted in Fig. 7a. High-resolution TEM (HRTEM) images (Fig. 7b and 7c) indicate that the (001) and (111) d-spacings of these NPs are 0.373 nm and 0.221 nm, respectively, which agree with the literature values. Fig. 7d shows the hysteresis loop measured at room temperature of nanoimprinted FePt NPs

as-prepared by pyrolysis of dot array nanopatterned metallopolymer blend. It reveals that the coercivity (H_c, a parameter indicative of magnetocrystalline anisotropy) of the nanodots is close to 0.38 T, which is satisfactory for practical data storage system at room temperature because the data can be manipulated easily by an external alternating magnetic field with a magnetic field strength realizable in typical magnetic data storage systems.[7] Similarly, $L1_0$ CoPt NPs have also been synthesized by one-step decomposition of heterobimetallic CoPt-containing metallopolymer (**P9**) or blend of Co-containing and Pt-containing homopolymers **P28** and **P17**.[22,38] The largest coercivity of the as-prepared $L1_0$ CoPt NPs is 0.54 T at 300 K.

The effect of pyrolysis temperature on the size and magnetic properties of the $L1_0$-FePt NPs was also investigated.[18] With higher pyrolysis temperature, smaller NPs with larger coercivity were obtained. This could be attributed to the improved crystallinity within each NP, which is a function of the pyrolysis temperature.

Table 1. Properties of some ferromagnetic metal alloy NPs

Metal alloy NPs	K_u [a] (10^7 erg cm^{-3})	M_s [b] (emu cm^{-3})	H_c [c] (kOe)	T_C [d] (K)
FePd ($L1_0$)	1.8	1100	33	760
CoPt ($L1_0$)	4.9	800	123	840
FePt ($L1_0$)	6.6-10	1140	116	750
CoPtCr	0.20	298	13.7	-
Co_3Pt	2.0	1100	36	-
MnAl	1.7	560	69	650
$Fe_{14}Nd_2B$	4.6	1270	73	585
$SmCo_5$	11-20	910	240-400	1000

[a] magnetocrystalline anisotropy; [b] saturation magnetization; [c] coercivity; [d] Curie temperature.

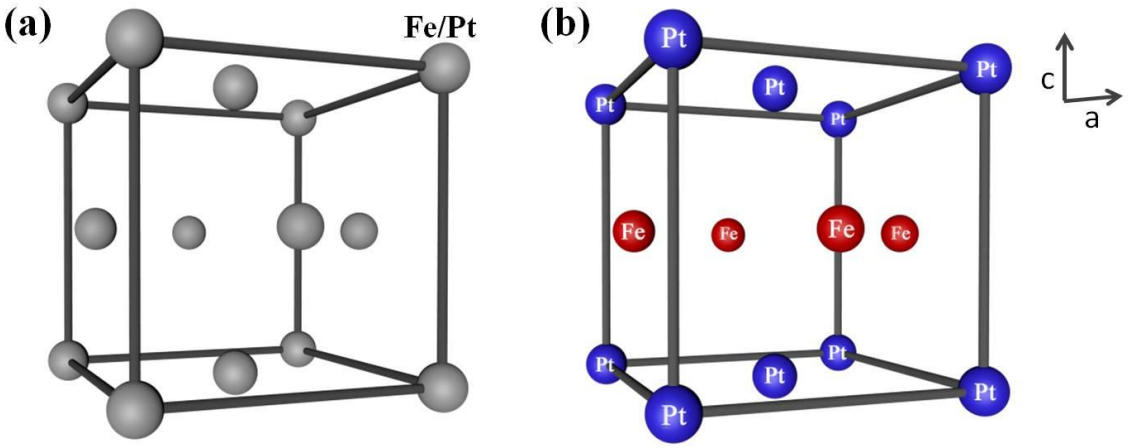

Fig. 6 Schematic illustration of the unit cell of (a) face-centered cubic (fcc or A_1) and (b) face-centered tetragonal (fct or $L1_0$) FePt NPs.

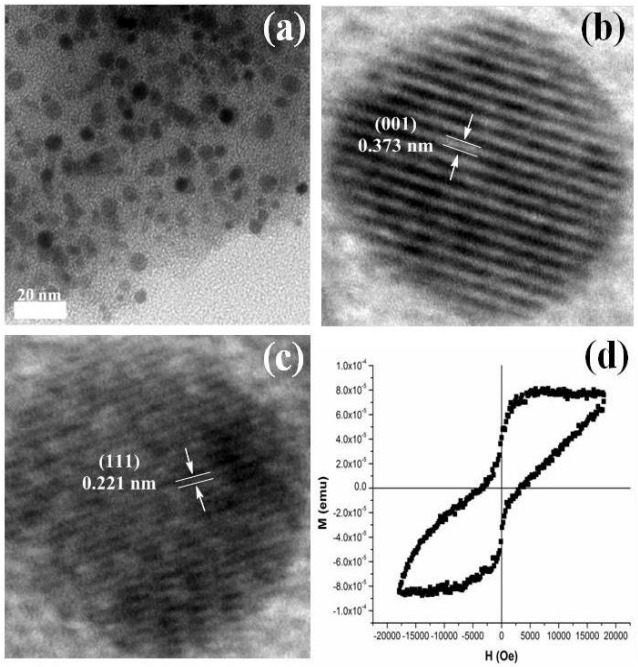

Fig. 7 (a) TEM and (b, c) HRTEM images of $L1_0$-FePt NPs as-synthesized from the metallopolymer blend; (d) hysteresis loop of the nanoimprinted FePt NPs as-prepared by pyrolysis of dot array nanopatterned metallopolymer blend. Reprinted with permission from ref. 29. Copyright (2014) Wiley-VCH.

3.3 CoFe NPs

Much effort was also devoted to preparing functional metallopolymers through ring-opening polymerization of the spirocyclic sila[1]ferrocenophane (e.g. PFSs, cobalt-clusterized PFSs (Co-PFS)) and magnetic metal/metal alloy ceramic films from these metallopolymers. Pyrolysis of **P10** afforded a high-yield ceramic (72% for 600 ^{o}C

and 59% for 900 °C) containing a high density of CoFe alloy NPs.[23] The magnetic properties of CoFe NPs can be easily tuned by varying the pyrolysis conditions, i.e., the ceramic prepared at 600 °C is superparamagnetic while that prepared at 900 °C is ferromagnetic or superparamagnetic with a blocking temperature > 355 K (Fig. 8).

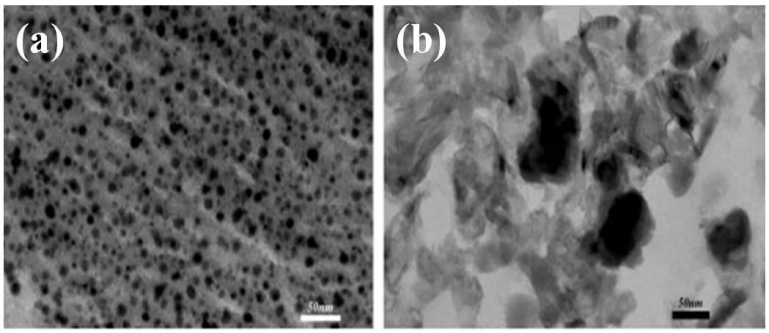

Fig. 8 TEM images of magnetic ceramics containing CoFe NPs prepared at (a) 600 °C and (b) 900 °C. Reprinted with permission from ref. 23. Copyright (2003) Wiley-VCH.

Liu *et al.* reported the pyrolysis of a highly metallized polymer precursor comprised of a PFS with pendant cobalt clusters under a reductive atmosphere (N_2/H_2 = 92%/8%), leading to magnetic CoFe NP-containing ceramic thin films.[10] They found that higher pyrolysis temperature yielded larger NPs with a broad size distribution at the surface of the resulting ceramic film, and the magnetic property was changed from superparamagnetic to ferromagnetic if the pyrolysis temperature was higher than 600 °C. In 2014, Tang and coworkers reported the preparation of CoFe-containing alloyed nanomaterials through pyrolyzing a series of cobaltocenium/ferrocene-containing heterobimetallic block copolymers (**P13**) at 800 °C in a reductive atmosphere of H_2/N_2 (5 v/v%) for 8 h. By varying the ratios of ferocene-containing block to cobaltocenium-containing block in the precursors, the as-generated NPs can change from metal phosphide to metal alloy nanomaterials (CoFe/carbon). The composition, morphology and magnetic properties of the resultant CoFe/carbon and

CoFe/phosphide/carbon nanomaterials were fully characterized by PXRD, TEM, inductively coupled plasma mass spectrometry (ICP-MS) and SQUID magnetometer (as shown in Fig. 9). It was confirmed that the CoFe NPs were ferromagnetic at room temperature and embedded in the carbon materials containing both amorphous carbon and carbon nanotubes, which can protect the NPs from oxidation or decomposition. Moreover, precursors with longer ferrocene-containing block showed lower blocking temperatures but higher magnetic saturation (as high as 212.0 emu g^{-1}).[6]

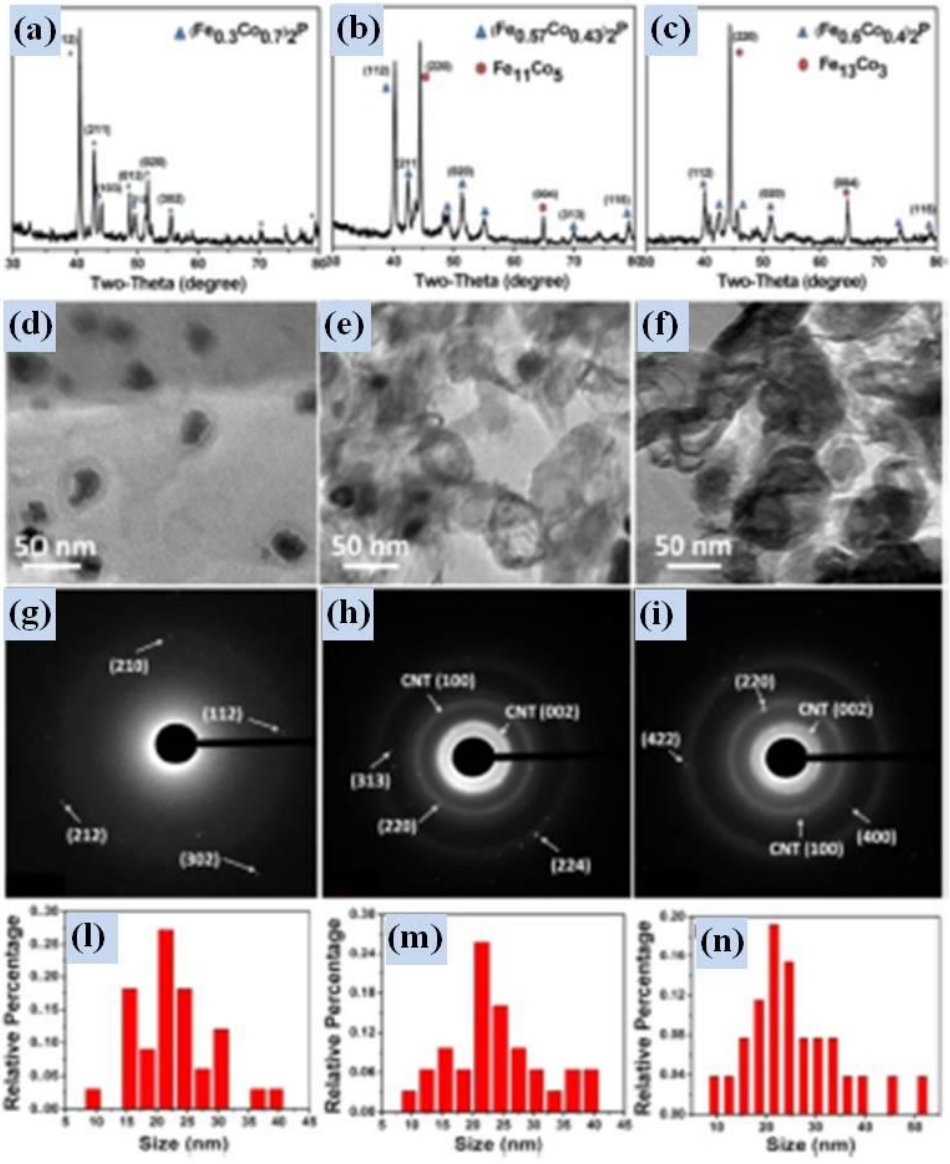

Fig. 9 (a-c) PXRD patterns, (b-f) TEM images, (g-i) selected area electron diffraction

(SAED) patterns, and (l-n) size distributions for NPs as-generated by thermal treatment of heterobimetallic block copolymers (**P13**) at 800 °C under a reductive atmosphere H_2/N_2 (5 v/v%). Reprinted with permission from ref. 6. Copyright (2014) American Chemical Society.

3.4 Fe or Co NPs

Pyrolysis of PFSs can generate magnetic ceramics containing α-Fe NPs in high yields, which allows fabrication of magnetic ceramic replicas from shaped PFS precursors on the nanometer scale.[25] For instance, the synthesis of magnetic ceramics containing α-Fe NPs was reported by the controlled pyrolysis of a series of PFSs, $[Fe(\eta^5\text{-}C_5H_4)_2(SiRR')]_n$ (R, R' = Me, Ph, H).[40] While all of these NPs are soft ferromagnetic, the α-Fe NPs as-synthesized at 600 °C are amorphous but those at 1000 °C are highly crystalline.

In 2004, Tang *et al.* described the generation of Co NPs by pyrolyzing *hb*-PYs-cobalt complex (**P27**) at high temperature. The resulting Co NPs exhibit high magnetic susceptibilities (saturation moment M_s up to ~118 emu g^{-1}) and low hysteresis losses (H_c down to ~0.045 kOe).[36] Moreover, by taking *hb*-PFPs-cobalt complex as the precursor, they fabricated magnetic ceramics containing both Fe and Co NPs by pyrolysis of the complex at 1000 °C. They also found that after incorporation of the Co NPs into the ceramics, the magnitude of their magnetization can be increased but the coercivity decreased from 0.35 kOe to 0.07 kOe.[25]

More recently, Gallei and co-workers reported the synthesis of magnetic core-shell nanorattles through thermal treatment of block copolymer poly(methyl methacrylate) –*b*-poly(2-(methacryloyloxy)-ethylferrocenecarboxylate) (PMMA-*b*-PFcMA), which is surface modified by trimethylethoxysilane (TMES). The surface coating of the

magnetic NPs with TMES can help avoid the agglomeration phenomenon which is often encountered in the traditional inorganic synthetic method.[14]

3.5 Others

In 2011, Thomas and co-workers presented the synthesis of ferromagnetic FePd metal alloy NPs by doping palladium(II) acetylacetonate or Pd NPs into poly(ferrocenylethylmethylsilane) (PFEMS) which subsequently underwent pyrolysis under argon at 1000 ^{o}C.[41] With the formation of these FePd alloy NPs, the coercivity, remanent magnetization and saturation magnetization of the resulting ceramics were enhanced. The synthesis of non-magnetic PtGe alloy NPs through a one-step pyrolytic treatment of **P16** was also reported.[30]

4 Fabrication of magnetic nanopatterned arrays

Lithography is a critical technique in the field of micro- and nano-processing and has been applied in many areas such as semiconductor, integrated circuits (ICs), microelectromechanical system (MEMS) devices, *etc*.[7,39] Table 2 shows the commonly used lithographic techniques and their capabilities.[42] Under electron beam and UV irradiation, most of the metallopolymers possess low etch rates due to the formation of protective layers of involatile metal ceramic compounds, which can therefore be used directly as a negative-tone resist to generate magnetic metallic nanostructures by electron-beam lithography (EBL) and UV photolithography (UVL).[10] Especially, by combining the merits of both the solution processability of metallopolymer and nanoimprint lithography (NIL), nanopatterns of ferromagnetic NPs can be generated in one step and in a large scale (1×1 cm^2) through pyrolysis of nanoimprinted

metallopolymers.[3] This would be utilized as the new platform for fabricating bit-patterned media (BPM) and next-generation of nanoscale ultra-high-density magnetic data storage devices. Furthermore, due to the different relative resistances to reactive ion etching (RIE) of the blocks, patterning of nanoscopic features with control over both periodicity and long-range order can also be achieved through self-assembly of metalloblock copolymers. Subsequent pyrolysis of nanopatterned metalloblock copolymers can afford well-defined nanoarrays of magnetic metal or metal alloy NPs *in situ* with periodicity down to dozens of nanometers. For instance, the polyferrocenylsilane-containing block copolymers are suitable for self-assembled nanolithography due to the presence of iron and silicon in the PFS block.

Table 2. Comparison of various lithographic techniques[42]

Lithographic methods	Electron beam lithography (EBL)	UV photolithography (UVL)	Focused ion beam lithography (FIBL)	Nanoimprint lithography (NIL)	Soft lithography	Dip-pen lithography	Self assembly
Minimum feature	≤ 5 nm	a few tens of nanometers	~10-20 nm	~5-10 nm	a few tens of nanometers	~ 10 nm	> 1 nm
Resolution	~ 10 nm	~ 90 nm	~ 30 nm	~ 5-10 nm	~ 30 nm	~ 20 nm	> 1 nm
Throughput	low	very high	very low	high	high	medium	low
Cost	high	low	very high	low	low	medium	low
Applications	masks, ICs, photonic crystals, *etc*.	MEMS devices, ICs, CPU chips, *etc*.	plasmonic lens	data storage, sensors, LOCs, nano channels, nano wires, *etc*.	LOCs	sensors	masks, ICs, data storage, *etc*.

4.1 Electron-beam lithography and UV photolithography

EBL is an attractive approach for the nanofabrication of metallic structures by direct-writing on a metallopolymer resist.[26,43] In 2005, metallic nanopatterns was fabricated by EBL with molybdenum-clusterized PFS (Mo-PFS) and nickel-clusterized PFS (Ni-PFS) as negative electron-beam resists, respectively (Fig. 10).[26] The polymer was first drop-coated onto a silicon substrate and then allowed to expose to an electron-beam. An optimal electron-beam dose of 25 mC cm^{-2} and 20 mC cm^{-2} was found for fabricating Mo-PFS and Ni-PFS, respectively, with uniformly patterned features and sufficient adhesion to the substrate following the pattern development in THF.

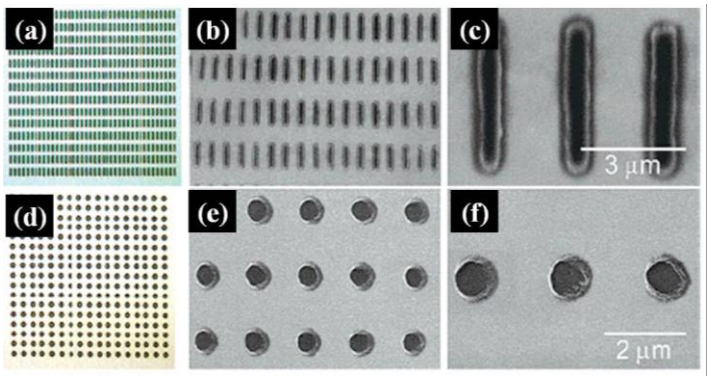

Fig. 10 (a) Optical micrographs and (b and c) scanning electron microscope (SEM) images of Mo-PFS microbars (0.5×4.0 μm^2), (d) optical micrography and (e and f) SEM images of Ni-PFS microdots (diameter = 1.0 μm). Images (e) and (f) were acquired with a 33º stage tilt. Reprinted with permission from ref. 26. Copyright (2005) American Chemical Society.

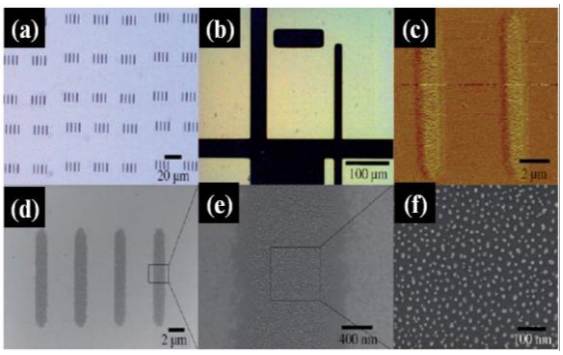

Fig. 11 Optical micrographs of **P2**: (a) microbars formed by EBL and (b) patterns

fabricated using UVL with a chrome contact mask. (c) MFM and (d–f) SEM images of microbars pyrolyzed at 500 ^{o}C under N_2. Reprinted with permission from ref. 2. Copyright (2008) Wiley-VCH.

UVL is a routine method for parallel patterning over large areas in microelectronics industry. The UVL patterning of Mo-PFS, Ni-PFS and Co-PFS was studied. Similar to EBL, the polymer was first pre-coated onto a silicon substrate and then allowed to expose to UV light (λ = 350−400 nm) through a chrome contact mask. Then, the desired patterns were developed in THF.[26]

In 2008, the nanopatterning of **P2** resist by EBL and UVL (Fig. 11a and 11b) was studied by a similar experimental procedure.[2] Pyrolysis of the patterned **P2** film under nitrogen gave FePt-NP patterns with excellent shape retention (Fig. 11c-11f), and the magnetic force microscopy (MFM) measurement confirms that these ceramic patterns are magnetic (Fig. 11c). This novel functionality of metallopolymers as negative resist to fabricate array patterns of magnetic NPs will offer much potential for incorporation into IC technology.

4.2 Nanoimprint lithography (NIL)

Traditional lithographic methods such as UVL only provide sub-micrometer resolution and EBL is not suitable for the fabrication of ordered nanostructured arrays of magnetic NPs over large areas owing to the restrictions of high cost, complicated procedures, and high demand of the materials. NIL is a low-cost and powerful technology for high-throughput patterning with high resolution. It has been used to imprint different kinds of polymers, allowing them wide applications in electronics, photonics, information storage and biotechnology.[44] By combining both the solution processability of **P3** and the soft NIL technique, nanoline and nanodot array patterns of

FePt-containing metallopolymers can be generated in one step.[3] From Fig. 12, a silicon substrate was first rinsed with acetone followed by deionized water coupled with sonication. Then, a saturated solution of **P3** in chloroform was drop-cast onto the substrate. A stamp made of polydimethylsiloxane (PDMS) was then used to imprint patterns onto the substrate with a constant and uniform force. The PDMS nanoimprint stamps used in such study include a line array nanopattern with periodicity (feature size) of 640 nm (350 nm) and a dot array nanopattern with periodicity (feature size) of 500 nm (250 nm). Exposing the sample to ultraviolet radiation (25 mW cm^{-2}, 391 nm) for 5 min presumably cross-linked the metallopolymer and transformed the FePt-containing polymer with low molecular weight into one with higher molecular weight. The chloroform solvent was evaporated in this step and left the mixed-metal polymer in the solid phase. Then, the PDMS mask was lifted from the substrate surface and a negative copy of the pattern was replicated to the FePt-based polymer on the sample surface. Next, the sample was dry etched with RIE to remove any residue in the trenches. This process takes advantage of the solubility of metallopolymers and imprints the polymer directly in the liquid phase, thereby eliminating the prior step of spinning and patterning the photoresist and the subsequent step of etching/lift-off of the FePt thin film. The metallopolymers were patterned at the nanoscale with high accuracy by the imprinting approach. Fig. 13 shows the SEM image of the imprinted polymer **P3** with nanoscale line and dot array patterns. Measurements of the line array periodicities and widths show high conformity of the final pattern to the imprint mold. The nanopatterned polymer can then be annealed to generate $L1_0$-FePt-NPs-based nanoline

and nanodot arrays (Fig. 13d and 13e) showing excellent pattern retention. Moreover, by taking the blend of **P17** and **P18**, nanodot array pattern was also achieved through the single-pot NIL.

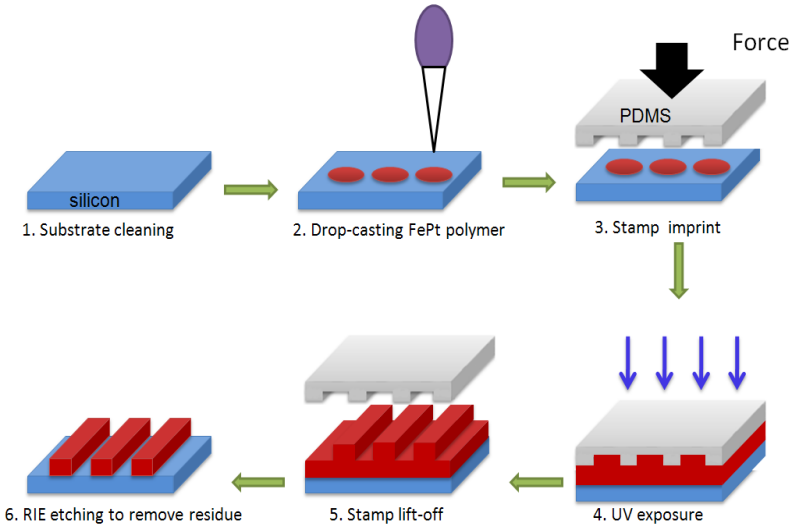

Fig. 12 Schematic illustration of the fabrication of large-area nanostructures from the metallopolymer by nanoimprinting. Reprinted with permission from ref. 3. Copyright (2012) Wiley-VCH.

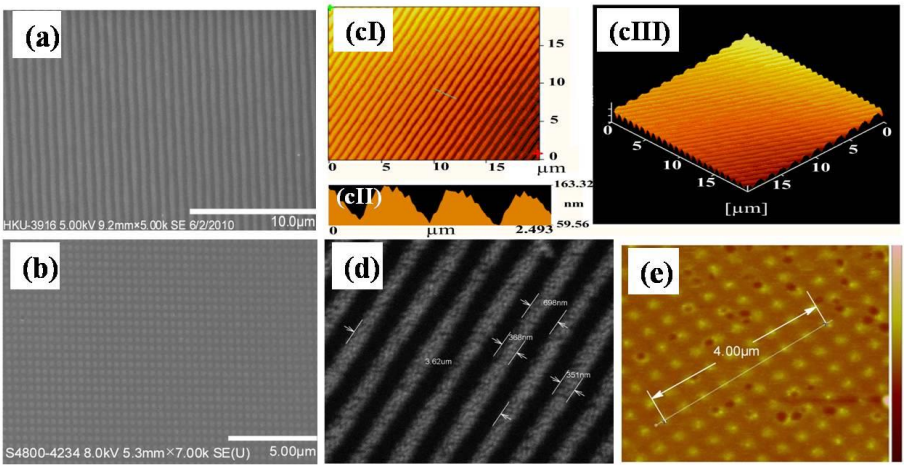

Fig. 13 SEM images of the nanoimprinted (a) line and (b) dot array patterns of **P3**. (c)(I) Topographic atomic force microscopy (AFM) image, (II) cross-section analysis and (III) 3D AFM image of the nanoimprinted line array pattern of **P3**. (d) SEM image and (e) AFM image of the nanoimprinted dot array FePt NPs after pyrolysis of **P3**. Reprinted with permission from ref. 3. Copyright (2012) Wiley-VCH.

A simple method to fabricate large-area highly ordered arrays of magnetic ceramic nanorods with precisely controllable dimensions and aspect ratios was reported in 2009 by nanoimprinting a high-molecular-weight PFS using anodic aluminum oxide (AAO)

templates.[45] Fig. 14 shows the SEM images of these PFS nanorods and their consequent ceramic nanorods prepared by pyrolysis at 700 ^{o}C for 5 h.

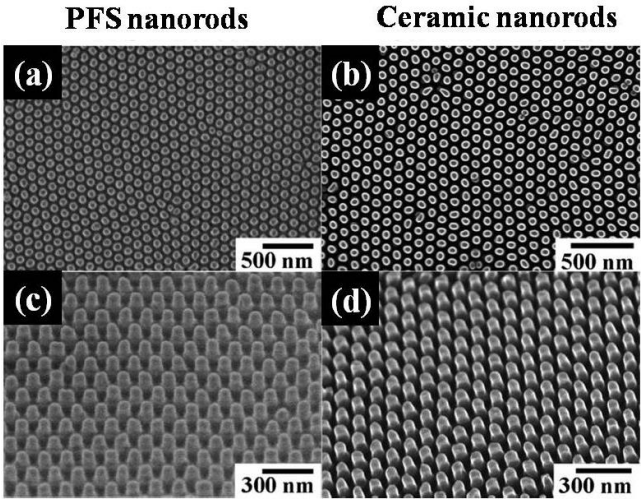

Fig. 14 SEM images of large-area highly ordered arrays of PFS nanorods and their consequent ceramic nanorods prepared by pyrolysis at 700 ^{o}C for 5 h: (a, b) top-view images and (c, d) angle view images. Reprinted with permission from ref. 45. Copyright (2009) American Chemical Society.

4.3 Self-assembly

The vast majority of block copolymers can undergo phase separation and then self-assemble into ordered nanodomains in solution due to the different chemical properties and low entropy of mixing of two blocks. For those block copolymers with crystallisable core-forming blocks, a variety of novel nanostructures can also be formed by crystallization-driven self-assembly *via* changing the solvent quality (normally by adding into the poor solvent of crystallizable core-forming block). The ability of block copolymers to self-assemble into ordered nanodomains have been widely used to fabricate nanostructures with periodicity down to several nanometers for applications in semiconductor devices, lithography, data recording systems, membranes, *etc*.[9,24] Self-assembly followed by controlled pyrolysis of metalloblock copolymers can produce patterned metal/metal alloy NPs *in situ* with periodicity down to dozens of

nanometers. The successful use of block copolymers in lithography requires a good etch selectivity between the blocks so that one or more of the blocks can be removed, leaving the morphology of the remaining block(s) undisturbed. PFS-containing block copolymers are quite useful in nanolithographic applications owing to the resistance properties of PFS block to oxygen RIE.[46] A series of PFS-containing multi-block copolymers such as PFS-*b*-PDMS, PFS-*b*-P2VP (P2VP = poly(2-vinylpyridine)), PFS-*b*-PMMA, PS-*b*-PFS-*b*-P2VP (PS = polystyrene), *etc.*, were used for self-assembled nanolithography.[47] For example, in the triblock copolymer PS-*b*-PFS-*b*-P2VP, the PS and P2VP can be removed easily using oxygen RIE, leaving the partly oxidized organometallic PFS shells intact.[46] The remaining PFS can be used as a mask for pattern transfer into functional materials. Fig. 15 shows the SEM images of the thin films of PS-*b*-PFS-*b*-P2VP on Si after annealing in chloroform and chloroform/acetone solvents for 4 h at room temperature, followed by oxygen RIE to remove the PS and P2VP.

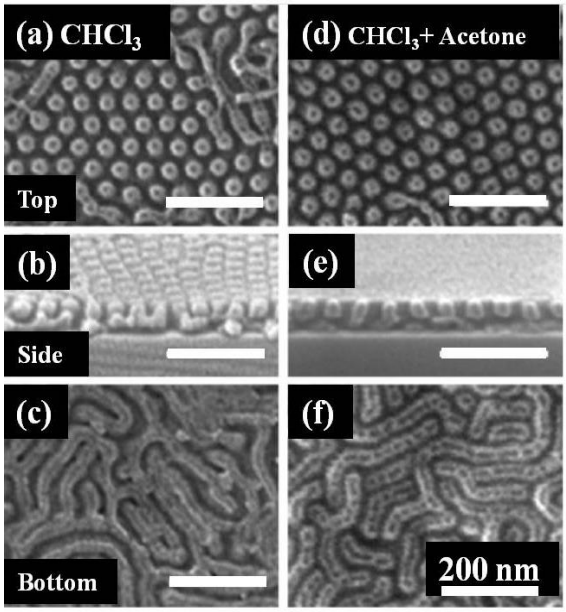

Fig. 15 SEM images of the thin films of PS-*b*-PFS-*b*-P2VP on Si after annealing in

different solvents for 4 h at room temperature, followed by etching with oxygen RIE to remove the PS and P2VP. (a, d) plane view. (b, e) side view. (c, f) bottom view. Reprinted with permission from ref. 46. Copyright (2009) Wiley-VCH.

Heterobimetallic block copolymers such as PFS_m-*b*-$([PCE][OTf])_n$ can also undergo self-assembly to give 3D cylindrical micelles with PFS_{34}-*b*-$P2VP_{272}$ as seed micelles.[24] By employing the solvent annealing approach, self-assembly of heterobimetallic block-random copolymers (**P12**) was achieved by drop-casting a 10 wt% chloroform solution into a Tefon mold by Tew and co-workers.[13] The morphologies of the resultant nanostructures were characterized by small-angle X-ray scattering (SAXS) and TEM (as shown in Fig. 16), indicating the formation of well-defined phase-separated nanodomains with cylindrical morphologies. The dark contrast of the cylindrical domain is attributed to the presence of the heavy Co and Fe atoms. The average diameter of the cylindrical domain (d_{cyl}) is around 20 nm and the average periodicity of the resultant nanopatterns is close to 47 nm.

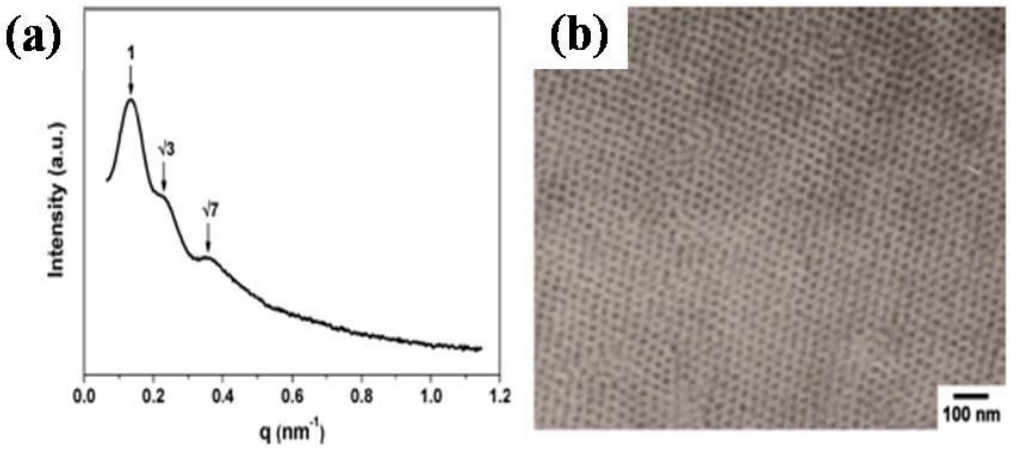

Fig. 16 (a) SAXS curve and (b) TEM image of a block random copolymer (**P12**) after solvent annealing in chloroform. Reprinted with permission from ref. 13. Copyright (2012) American Chemical Society.

5 Applications

5.1 Magnetic data storage

Ordered arrays of magnetic nanostructures have attracted intense academic and industrial interest, due to their widespread technological applications in areas such as biosensors, spintronics, IC, MRAM and patterned recording media.[1,7] Direct and rapid fabrication of bit-patterned $L1_0$-FePt nanostructure is a crucial challenge for exploiting $L1_0$-FePt NPs in ultra-high-density data storage system. As aforementioned, nanopatterns of $L1_0$-FePt NPs can be fabricated from **P3** through NIL. The as-generated nanopatterns of $L1_0$-FePt NPs possess a room-temperature coercivity as large as 1.4 T (i.e. 14 kOe) which is comparable to those values of the magnetic recording media currently in use.[3] From the MFM images of the nanodot patterns, the magnetization directions of the patterned $L1_0$-FePt NPs can be adjusted to show "up" or "down" by controlling an external magnetic field, and this proof-of-principle demonstration can provide a new platform for BPM and next-generation nanoscale high-density magnetic data storage devices (Fig. 17). Table 3 shows the relationship of the pitch size and areal density of BPM. If one can generate a BPM with a pitch size of 25 nm, the areal density can reach 1 Tbit in^{-2}. Since the NIL can offer sub-5 nm patterning resolution over large areas, these FePt-based metallopolymers in conjunction with NIL can offer an alternative route for obtaining BPM with the storage density a few times higher than the current harddisk technology, without resorting to the use of some sophisticated fabrication techniques.

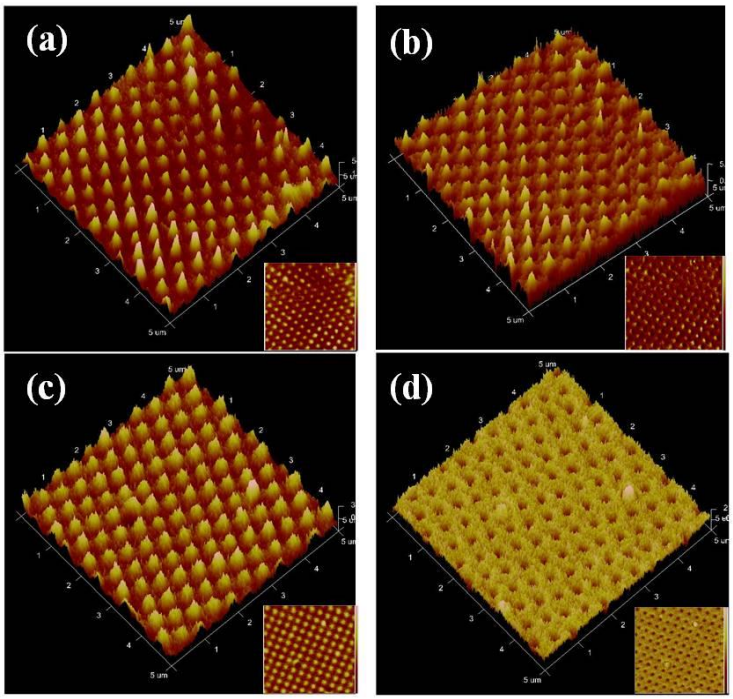

Fig. 17 (a) AFM image and (b) MFM image of the nanoimprinted dot array pattern of FePt NPs field-annealed in the –Z magnetic direction with a periodicity of ~500 nm and feature size of ~250 nm. (c) AFM image and (d) MFM image of the nanoimprinted dot array pattern of FePt NPs field-annealed in the +Z direction with the same periodicity and feature size. Reprinted with permission from ref. 3. Copyright (2012) Wiley-VCH.

Table 3. Relationship of the pitch size and areal density of BPM.

Pitch size (nm)	Bit size (nm) (Half-pitch)	Areal density (Tbit in^{-2})
35	17.5	0.5
30	15.0	0.72
25	12.5	1
21	10.5	1.5
18	9.0	2.0
8	4.0	10

5.2 Functional ceramic films

The use of RIE with metallopolymers as resists to form metal-containing ceramic materials with interesting physical properties is highly intriguing. By taking Co-PFS as the precursor, the facile fabrication of ferromagnetic ceramic films containing

metal-rich nanoworm networks derived from O_2-RIE of the thin films of Co-PFS in a secondary magnetic field was reported (Fig. 18).[43] The patterning of highly metallized metallopolymer resists using soft lithographic techniques combined with RIE in a secondary magnetic field can produce ordered arrays of ferromagnetic ceramics that may find applications in spintronics and logic circuits. The synthesis of superparamagnetic ceramic film containing Fe NPs with controlled size was studied through the pyrolysis of **P13** in the ordered channels of the mesoporous silica (MCM-41).[48]

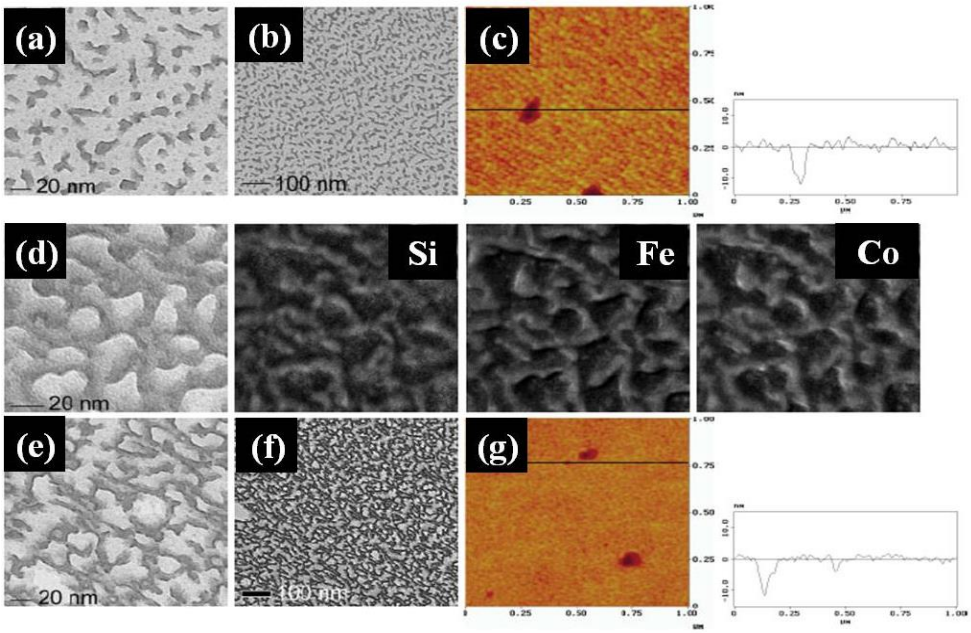

Fig. 18 (a, b)TEM images of a magnetic film following O_2-RIE with (c) tapping-mode AFM image of a thin film on a Si substrate under similar conditions with sectional analysis (right). (d) TEM image of the same film with electron energy loss spectroscopy (EELS) elemental maps for Si, Fe, and Co. (e, f) TEM images of a magnetic film following H_2-RIE with (g) tapping-mode AFM image of a thin film on Si under similar conditions with sectional analysis (right). Reprinted with permission from ref. 43. Copyright (2004) Wiley-VCH.

5.3 Optimization of organic light-emitting diodes with magnetic alloy NPs

Organic light-emitting diodes (OLEDs) have attracted widespread attention in recent years due to the promising commercial applications in flat panel displays, solid-

state lighting, virtual reality, *etc*.[49,50] However, there are still big challenges in achieving satisfactory efficiency and lifetime of the devices. After numerous efforts were made in the last decade, nearly 100% internal quantum efficiency of OLEDs has been achieved. However, the external quantum efficiency (EQE) is still very low, which limits their commercial applications to a large extent. The key problem of low EQE is the poor light extraction efficiency. Light extraction efficiency in conventional OLEDs is only 20%, and the other 80% of the emitted light is lost through the waveguide (WG) mode, substrate mode, electrode absorption, and/or localized surface plasmons (LSPs) at the metal electrode-organic interface. The efficient light out-coupling enhancement in OLEDs via simultaneous LSPs excitation and light scattering effect using Pt_3Co alloy NPs has been reported by Tang *et al*.[49] More recently, the surface carbon-coated $L1_0$ FePt and CoPt alloy NPs made from metallopolymer precursors can be incorporated in the hole-transport layers (HTLs) of OLEDs to improve the device performance, Fig. 19a depicts the structure of the doped device.[50] Doped green OLEDs at 0.05 wt.% FePt and CoPt NPs gave the best performance. As seen from Fig. 19b, the electroluminescent (EL) intensity of OLEDs doped with FePt and CoPt alloy NPs increased considerably with increasing current density. Eventually, significant improvements of ~47.1% (0.05 wt.% FePt doped green OLED) and 48.5% (0.05 wt.% CoPt doped green OLED) in the EL efficiency were achieved, respectively (Fig. 19c). Through detailed investigations of the mechanism underlying the improvement, it was found that the presence of an alloy NPs-incorporated poly(3,4-ethylenedioxythiophene):polystyrene sulfonate (PEDOT:PSS) HTL actually

acts as an optical outcoupling layer contributing to the efficiency enhancement, accomplished by the collective effects of light-scattering, LSP resonance and increased electron trap density induced by magnetic metal alloy NPs. The introduction of magnetic metal alloy NPs in the devices does not change the shape of EL spectra, implying the high EL stability of doped OLEDs (Fig. 19d). Moreover, the particle size, doping concentration and magnetic property of metal alloy NPs play important roles in the performance optimization of OLEDs.

Introduction of Pt-based magnetic alloy NPs to form composite organic/inorganic HTLs is proved to be an effective way to improve light out-coupling in OLEDs and other similar light-emitting devices. Additionally, by comparing with the reported method,[46] the amount of magnetic alloy NPs incorporated in the HTL is much less and the operation procedures are much simpler, which implies that this method is a more commercially viable approach for industrial application.[49]

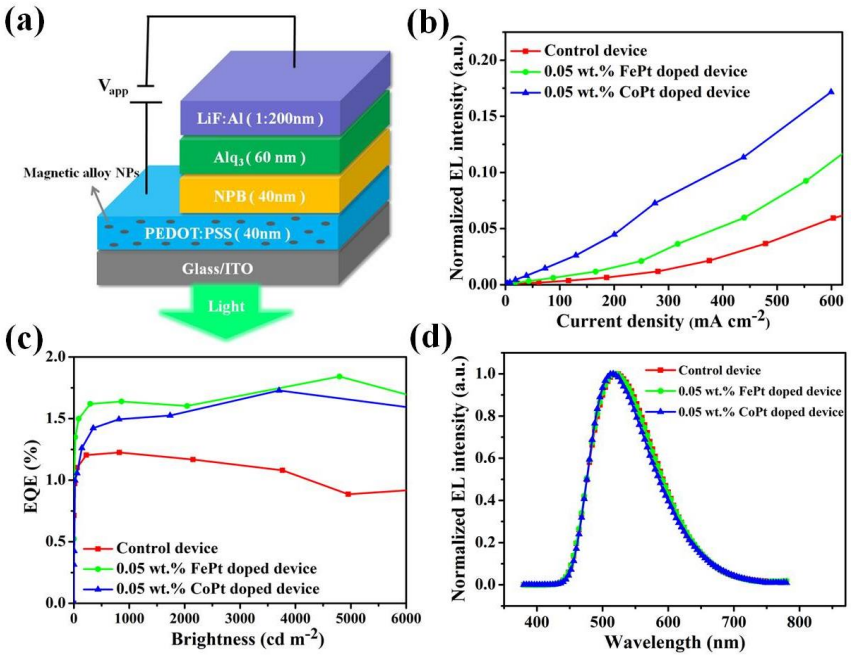

Fig. 19 (a) Schematic drawing illustrating the device structure of OLEDs with a PEDOT:PSS/magnetic NPs hybrid HTL, (b) relative EL intensity versus current density,

(c) EQE versus brightness, and (d) normalized EL spectra characteristics measured for the control device, FePt doped, and CoPt doped devices.

6 Conclusions and future perspectives

An overview on the development of using metallopolymers as precursors to generate functional magnetic metal/metal alloy NPs and other nanostructures by controlled pyrolysis is provided here. Through rational molecular design and appropriate polymerization methods, mononuclear metallic or heterobimetallic polymers with metal elements on the side and/or main chain can be generated smoothly. The structure of metallopolymer and the pyrolyzing condition can significantly influence the size, composition and properties of the resultant magnetic ceramic NPs. By comparison to the traditional synthetic approach, preparation of ferromagnetic alloy NPs ($L1_0$ FePt and CoPt, *etc.*) from metallopolymer precursors is very attractive because it can avoid the step of post-annealing treatment. Moreover, most of the metallopolymers can act as the negative tone resist for the fabrication of the nanopatterned magnetic metal/metal alloy NPs through various lithographic techniques. Self-assembly followed by pyrolysis or solvent annealing of the metalloblock copolymers can form nanopatterns *in situ* with periodicity down to dozens of nanometers. The patterned functional metallopolymer precursors and patterned arrays of magnetic nanocomposites hold great promise for applications in high-density data storage media and spintronic devices. However, there are still some limitations and challenges remaining unresolved in this research area. For example, the controlled synthesis of heterobimetallic polymers with desirable solubility is still very difficult and needs to be further addressed. *In situ* generation of ferromagnetic alloy NPs

through self-assembly of metalloblock copolymers is also not easily achieved, because both the precise control of phase-separation and introduction of specific metal elements in each block is very challenging. Moreover, the relationship of the particle size, composition and shape of NPs with the metal center environment in the polymer backbone, as well as the nucleation mechanism of metal-based NPs are also not yet clear and need to be addressed in the future. The effects of pyrolyzing parameters (such as temperature, heating ramp, heating duration, atmosphere, *etc*.) on the magnetic properties of as-generated NPs are also needed to be scrutinized and certified. Finally, the creation of ultra-high-density data storage or spintronic devices based on patterned arrays of magnetic NPs is still not yet explored, which is very desirable for the current big data era. Despite these obstacles, it is obvious that the approach of using metallopolymer precursors for making functional metal-based nanocomposites is very attractive because of their unique solution processability, film-forming property as well as precise control of the size and composition of the resulting NPs. For example, a novel approach to synthesize conducting polymer/semiconductor NP hybrid materials was developed based on the seeded growth of NPs within conducting metallopolymers. The use of metalloporphyrin templates toward the preparation of other metal alloy NPs is also worthy of study.[21,22] It is noteworthy that the application of magnetic NPs in biomedicine is very intriguing, which has already developed to be a hot spot in the multidisciplinary research of nanomaterials, chemistry, biology and medicine. Therefore, it is stimulating to explore the application of magnetic nanomaterials as prepared from metallpolymer precursors in the biomedicine field.

While the full potential of metallopolymers as precursors for the generation of functional metal-based nanocomposites is not yet fully exploited, this venture will definitely inspire scientists in both academic institutes and industry to make further breakthroughs along this direction in the near future.

Abbreviations

Anodic aluminum oxide (AAO)
Atom transfer radical polymerization (ATRP)
Atomic force microscopy (AFM)
Bit-patterned media (BPM)
Cobalt-clusterized PFSs (Co-PFS)
Coercivity (H_c)
Curie temperature (T_C)
Differential scanning calorimetry (DSC)
Electroluminescenc (EL)
Electron-beam lithography (EBL)
Electron energy loss spectroscopy (EELS)
Electron-beam lithography (EBL)
Electroluminescent (EL)
Elemental analysis (EA)
Energy-dispersive X-ray (EDX)
External quantum efficiency (EQE)
Face-centered cubic (fcc)
Face-centered tetragonal (fct)
Focused ion beam lithography (FIBL)
Gel permeation chromatography (GPC)
Glass-transition temperature (T_g)
High-resolution transmission electron microscopy (HRTEM)
Hole-transport layers (HTLs)
Hyperbranched polyynes (hb-PYs)
Inductively coupled plasma mass spectrometry (ICP-MS)
Infrared (IR)
Integrated circuit (IC)
Lab-on-a-chip (LOC)
Localized surface plasmons (LSPs)
Magnetic force microscopy (MFM)

Magnetic nanoparticles (MNPs)
Magnetic random access memory (MRAM)
Magnetic resonance imaging (MRI)
Magnetic anisotropy constant or magnetocrystalline anisotropy (K_u)
Microelectromechanical system (MEMS)
Molybdenum-clusterized PFS (Mo-PFS)
Nanoimprint lithography (NIL)
Nanoparticles (NPs)
Nickel-clusterized PFS (Ni-PFS)
Nuclear magnetic resonance (NMR)
Organic light-emitting diodes (OLEDs)
Onset decomposition temperature (T_{decomp})
Poly(cobaltoceniumethylene) (PCE)
Polydimethylsiloxane (PDMS)
Poly(3,4-ethylenedioxythiophene):polystyrene sulfonate (PEDOT:PSS)
Poly(ferrocenylethylmethylsilane) (PFEMS)
Poly(ferrocenylphenylenes) (hb-PFPs)
Polyferrocenylsilane (PFS)
Poly(2-(methacryloyloxy)-ethylferrocenecarboxylate) (PFcMA)
Poly(methyl methacrylate) (PMMA)
Poly(*p*-phenyleneethynylene) (PPE)
Poly(2-vinylpyridine) (P2VP)
Polystyrene (PS)
Powder X-ray diffraction (PXRD)
Reactive ion etching (RIE)
Remnant magnetic moment (M_r)
Reversible-addition-fragmentation chain transfer (RAFT)
Ring-opening metathesis polymerization (ROMP)
Ring-opening polymerization (ROP)
Scanning electron microscope (SEM)
Saturation magnetization (M_s)
Selected area electron diffraction (SAED)
Small-angle X-ray scattering (SAXS)
Superconducting quantum interference device (SQUID)
Thermal gravimetric analysis (TGA)
Transmission electron microscopy (TEM)
Trimethylethoxysilane (TMES)
Ultraviolet-visible (UV-vis)
UV photolithography (UVL)

Vibrating sample magnetometry (VSM)
Waveguide (WG)
X-ray magnetic circular dichroism (XMCD)

Acknowledgements

Q. Dong and Z. Meng contributed equally to this work. We acknowledge the financial support from the National Natural Science Foundation of China (61774109, 51573151, 21504074), Areas of Excellence Scheme of HKSAR (AoE/P-03/08), Hong Kong Research Grants Council (HKBU12302114 and PolyU123172/16P), Hong Kong Polytechnic University (1-ZE1C) and the Shenzhen Basic Research Program of the Science, Technology and Innovation Committee of Shenzhen Municipality (JCYJ20160531193836532 and JCYJ20170303160036674). W.-Y. Wong also acknowledges Ms. Clarea Au for the Endowed Professorship in Energy (847s). Q. Dong also thanks the financial support from the Youth "Sanjin" Scholar Program and the Key R&D Project of Shanxi Province (International Cooperation Program, project No. 201603D421032).

References

1 A.-H. Lu, E. L. Salabas and F. Schth, *Angew. Chem. Int. Ed*., 2007, **46**, 1222–1244.
2 K. Liu, C.-L. Ho, S. Aouba, Y. Q. Zhao, Z. H. Lu, S. Petrov, N. Coombs, P. Dube, H. E. Ruda, W.-Y. Wong and I. Manners, *Angew. Chem. Int. Ed*., 2008, **47**, 1255–1259.
3 Q. Dong, G. Li, C.-L. Ho, M. Faisal, C.-W. Leung, P. W.-T. Pong, K. Liu, B.-Z. Tang, I. Manners and W.-Y. Wong, *Adv. Mater*., 2012, **24**, 1034–1040.
4 N. A. Frey, S. Peng, K. Cheng and S. Sun, *Chem. Soc. Rev*., 2009, **38**, 2532–2542.
5 K. D. Gilroy, A. Ruditskiy, H.-C. Peng, D. Qin and Y. Xia, *Chem. Rev.*, 2016, **116**, 10414–10472.
6 J. Zhang, Y. Yan, J. Chen, W. M. Chance, J. Hayat, Z. Gai and C. Tang, *Chem. Mater.*, 2014, **26**, 3185–3190.

7 J. P. Wang, *IEEE*, 2008, **96**, 1847–1863.
8 I. Robinson, S. Zacchini, L. D. Tung, S. Maenosono and N. T. K. Thanh, *Chem. Mater.*, 2009, **21**, 3021–3026.
9 L. Zhao, X. Liu, L. Zhang, G. Qiu, D. Astruc and H. Gu, *Coord. Chem. Rev.*, 2017, **337**, 34–79.
10 K. Liu, S. B. Clendenning, L. Friebe, W. Y. Chan, X. Zhu, M. R. Freeman, G. C. Yang, C. M. Yip, D. Grozea, Z. H. Lu and I. Manners, *Chem. Mater*., 2006, **18**, 2591–2601.
11 W.-Y. Wong and C.-L. Ho, *Acc. Chem. Res*., 2010, **43**, 1246–1256.
12 G. Mera, M. Gallei, S. Bernard and E. Ionescu, *Nanomaterials*, 2015, **5**, 468–540.
13 Y. Zha, H. D. Thaker, R. R. Maddikeri, S. P. Gido, M. T. Tuominen and G. N. Tew, *J. Am. Chem. Soc.*, 2012, **134**, 14534–14541.
14 D. Scheid, D. Stock, T. Winter, T. Gutmann, C. Dietz and M. Gallei, *J. Mater. Chem. C*, 2016, **4**, 2187–2196.
15 R. H. Staff, M. Gallei, M. Mazurowski, M. Rehahn, R. Berger, K. Landfester and D. Crespy, *ACS Nano*, 2012, **6**, 9042–9049.
16 G.-J. Zhou and W.-Y. Wong, *Chem. Soc. Rev*., 2011, **40**, 2541–2566.
17 Y. Lu, N. Yeung, N. Sieracki and N. M. Marshall, *Nature*, 2009, **460**, 855–862.
18 Q. Dong, G. Li, H. Wang, P. W.-T. Pong, C. W. Leung, I. Manners, C.-L. Ho, H. Li and W.-Y. Wong, *J. Mater. Chem. C*, 2015, **3**, 734–741.
19 Z. Meng, G. Li, H.-F. Wong, S.-M. Ng, S.-C. Yiu, C.-L. Ho, C.-W. Leung, I. Manners and W.-Y. Wong, *Nanoscale*, 2017, **9**, 731–738.
20 Z. Meng, G. Li, H.-F. Wong, S.-M. Ng, S.-C. Yiu, C.-L. Ho, C.-W. Leung and W.-Y. Wong, *Polym. Chem*., 2016, **7**, 4467–4475.
21 Q. Dong, W. Qu, W. Liang, F. Tai, K. Guo, C.-W. Leung and W.-Y. Wong, *J. Mater. Chem. C*, 2016, **4**, 5010–5018.
22 Q. Dong, W. Qu, W. Liang, K. Guo, H. Xue, Y. Guo, Z. Meng, C.-L. Ho, C.-W. Leung and W.-Y. Wong, *Nanoscale*, 2016, **8**, 7068–7074.
23 A. Berenbaum, M. Ginzburg-Margau, N. Coombs, A. J. Lough, A. Safa-Sefat, J. E. Greedan, G. A. Ozin and I. Manners, *Adv. Mater*., 2003, **15**, 51–55.
24 J. B. Gilroy, S. K. Patra, J. M. Mitchels, M. A. Winnik and I. Manners, *Angew. Chem. Int. Ed*., 2011, **50**, 5851–5855.
25 J. Shi, B. Tong, Z. Li, J. Shen, W. Zhao, H. Fu, J. Zhi,Y. Dong, M. Häussler, J. W. Y. Lam and B. Z. Tang, *Macromolecules*, 2007, **40**, 8195–8204.
26 W. Y. Chan, S. B. Clendenning, A. Berenbaum, A. J. Lough, S. Aouba, H. E. Ruda and I. Manners, *J. Am. Chem. Soc*., 2005, **127**, 1765–1772.
27 M. Erhard, K. Lam, M. Haddow, G. R. Whittell, W. E. Geiger and I. Manners, *Polym. Chem*., 2014, **5**, 1264–1274.
28 C.-L. Ho, S.-Y. Poon, K. Liu, C.-K. Wong, G.-L. Lu, S. Petrov, I. Manners and

W.-Y. Wong, *J. Organomet. Chem*., 2013, **744**, 165–171.
29 Q. Dong, G. Li, C.-L. Ho, C.-W. Leung, P. W.-T. Pong, I. Manners and W.-Y. Wong, *Adv. Funct. Mater*., 2014, **24**, 857–862.
30 W. Bian, H. Lian, Y. Zhang, F. Tai, H. Wang, Q. Dong, B. Yu, X. Wei and Q. Zhao, *J. Organomet. Chem*., 2017, **835**, 25–30.
31 V. Bellas and M. Rehahn, *Angew. Chem. Int. Ed*., 2007, **46**, 5082–5104.
32 K. Kulbaba and I. Manners, *Macromol. Rapid Commun*., 2001, **22**, 711–724.
33 S. Baljak, A. D. Russell, S. C. Binding, M. F. Haddow, D. O'Hare and I. Manners, *J. Am. Chem. Soc*., 2014, **136**, 5864–5867.
34 A. Berenbaum and I. Manners, *Dalton Trans*., 2004, 2057–2058.
35 S. Scholz, P. J. Leech, B. C. Englert, W. Sommer, M. Weck and U. H. F. Bunz, *Adv. Mater*., 2005, **17**, 1052–1055.
36 M. Häussler, R. Zheng, J. W. Y. Lam, H. Tong, H. Dong and B. Z. Tang, *J. Phys. Chem. B*, 2004, **108**, 10645–10650.
37 B. Jiang, W. L. Hom, X. Chen, P. Yu, L. C. Pavelka, K. Kisslinger, J. B. Parise, S. R. Bhatia and R. B. Grubbs, *J. Am. Chem. Soc*., 2016, **138**, 4616–4625.
38 T. Gong, Z. Gao, W. Bian, F. Tai, W. Liang, W. Liang, Q. Dong and C. Dong, *J. Organomet. Chem*., 2016, **819**, 237–241.
39 D. Weller and M. F. Doerner, *Annu. Rev. Mater. Sci.*, 2000, **30**, 611–644.
40 R. Petersen, D. A. Foucher, B. Z. Tang, A. Lough, N. P. Raju, J. E. Greedan and I. Manners, *Chem. Mater*., 1995, **7**, 2045–2053.
41 K. R. Thomas and E. Sivaniah, *J. Appl. Phys*., 2011, **109**, 0739041–8.
42 A. Pimpin and W. Srituravanich, *Eng. J*., 2012, **16**, 37−55.
43 S. B. Clendenning, S. Han, N. Coombs, C. Paquet, M. S. Rayat, D. Grozea, P. M. Brodersen, R. N. S. Sodhi, C. M. Yip, Z. H. Lu and I. Manners, *Adv. Mater*., 2004, **16**, 291–296.
44 L. J. Guo, *Adv. Mater*., 2007, **19**, 495–513.
45 K. Liu, S. Fournier-Bidoz, G. A. Ozin and I. Manners, *Chem. Mater*., 2009, **21**, 1781–1783.
46 V. P. Chuang, C. A. Ross, J. Gwyther and I. Manners, *Adv. Mater*., 2009, **21**, 3789–3793.
47 N. McGrath, F. H. Schacher, H. Qiu, S. Mann, M. A. Winnik and I. Manners, *Polym. Chem*., 2014, **5**, 1923–1929.
48 M. J. MacLachlan, M. Ginzburg, N. Coombs, N. P. Raju, J. E. Greedan, G. A. Ozin and I. Manners, *J. Am. Chem. Soc*., 2000, **122**, 3878–3891.
49 Y. Gu, D. Zhang, Q. Ou, Y. Deng, J. Zhu, L. Cheng, Z. Liu, S.-T. Lee, Y. Li and J. Tang, *J. Mater. Chem. C*, 2013, **1**, 4319−4326.
50 Q. Dong, F. Tai, H. Lian, B. Zhao, Z. Zhong, Z. Chen, J. X. Tang and F. R. Zhu, *Nanoscale*, 2017, **9**, 2875–2882.